

Article

Effect of PLGA Concentration in Electrospinning Solution on Biocompatibility, Morphology and Mechanical Properties of Nonwoven Scaffolds

Arsalan D. Badaraev ¹, Tuan-Hoang Tran ¹, Anastasia G. Drozd ¹, Evgenii V. Plotnikov ^{1,2},
Gleb E. Dubinenko ¹, Anna I. Kozelskaya ¹, Sven Rutkowski ^{1,*} and Sergei I. Tverdokhlebov ^{1,*}

- ¹ Weinberg Research Center, School of Nuclear Science & Engineering, National Research Tomsk Polytechnic University, 30 Lenin Avenue, 634050 Tomsk, Russia; adb6@tpu.ru (A.D.B.); cungbinh9327@gmail.com (T.-H.T.); agd7@tpu.ru (A.G.D.); plotnikovev@tpu.ru (E.V.P.); dubinenko.gleb@gmail.com (G.E.D.); kozelskayaai@tpu.ru (A.I.K.)
- ² Mental Health Research Institute, Tomsk National Research Medical Center of the Russian Academy of Sciences, Aleutskaya Street 4, 634014 Tomsk, Russia
- * Correspondence: rutkowski_s@tpu.ru (S.R.); tverd@tpu.ru (S.I.T.)

Abstract: In this work, the effects of weight concentration on the properties of poly(lactide-co-glycolide) polymeric scaffolds prepared by electrospinning are investigated, using four different weight concentrations of poly(lactide-co-glycolide) for the electrospinning solutions (2, 3, 4, 5 wt.%). With increasing concentration of poly(lactide-co-glycolide) in the electrospinning solutions, their viscosity increases significantly. The average fiber diameter of the scaffolds also increases with increasing concentration. Moreover, the tensile strength and maximum elongation at break of the scaffold increase with increasing electrospinning concentration. The prepared scaffolds have hydrophobic properties and their wetting angle does not change with the concentration of the electrospinning solution. All poly(lactide-co-glycolide) scaffolds are non-toxic toward fibroblasts of the cell line 3T3-L1, with the highest numbers of cells observed on the surface of scaffolds prepared from the 2-, 3- and 4-wt.% electrospinning solutions. The results of the analysis of mechanical and biological properties indicate that the poly(lactide-co-glycolide) scaffolds prepared from the 4 wt.% electrospinning solution have optimal properties for future applications in skin tissue engineering. This is due to the fact that the poly(lactide-co-glycolide) scaffolds prepared from the 2 wt.% and 3 wt.% electrospinning solution exhibit low mechanical properties, and 5 wt.% have the lowest porosity values, which might be the cause of their lowest biological properties.

Keywords: electrospinning; PLGA scaffolds; polymer concentration; biocompatibility; degradation



Citation: Badaraev, A.D.; Tran, T.-H.; Drozd, A.G.; Plotnikov, E.V.; Dubinenko, G.E.; Kozelskaya, A.I.; Rutkowski, S.; Tverdokhlebov, S.I. Effect of PLGA Concentration in Electrospinning Solution on Biocompatibility, Morphology and Mechanical Properties of Nonwoven Scaffolds. *Technologies* **2023**, *11*, 137. <https://doi.org/10.3390/technologies11050137>

Academic Editors: Yury A. Skorik and Eugene Wong

Received: 31 July 2023

Revised: 8 September 2023

Accepted: 29 September 2023

Published: 5 October 2023



Copyright: © 2023 by the authors. Licensee MDPI, Basel, Switzerland. This article is an open access article distributed under the terms and conditions of the Creative Commons Attribution (CC BY) license (<https://creativecommons.org/licenses/by/4.0/>).

1. Introduction

Electrospun scaffolds have become of great interest for tissue engineering applications in recent decades [1]. Their porous structure and high porosity-to-volume ratio impart electrospun scaffolds their superior suitability for tissues regeneration, tissue barrier, and drug delivery [2–4]. An important advantage of electrospun scaffolds is their ability to be tailored across a wide range of porosity and morphology. The desired porosity of the scaffold and the morphology of the individual fibers could be precisely tailored by the parameters of the electrospinning process and the composition of the electrospinning solution. While parameters of the electrospinning process affect the morphology of the scaffold, the selection of the composition of the electrospinning solution largely determines both the morphology and the final properties of the scaffold [5].

Due to their biodegradability and biocompatibility, synthetic aliphatic polyesters have found numerous applications in tissue engineering [6–8]. One of them is the aliphatic block copolymer poly(lactic-co-glycolic acid) (PLGA), which consists of the monomers lactic

acid and glycolic acid. PLGA is one of the most commonly used biodegradable synthetic polymers in tissue engineering [6]. The US Food and Drug Administration has approved the use of PLGA in clinical cases [6]. Like other biodegradable synthetic polymers, PLGA possesses good biocompatibility and mechanical behavior [9]. A particular advantage of PLGA is the ability to control the degradation rate by altering the mixing ratio of the monomers lactic acid and glycolic acid in the polymer being synthesized.

Electrospinning is actively used to fabricate highly porous, biocompatible and mechanically stable polymeric scaffolds consisting of chaotically interwoven nanofibers with diameters ranging from several nanometers to microns [10]. Electrospinning can fabricate a polymeric scaffold with a structure that provides a suitable topology (extracellular matrix structure) for the extracellular matrix of cells [11]. This extracellular matrix structure is optimal for cell proliferation, migration and differentiation, which is why attempts are being made to fabricate biocompatible materials with the most similar design [12,13]. PLGA scaffolds fabricated by electrospinning are also being studied for this purpose and are being used in biomedicine for the regeneration of neural [14], periodontal [15], bone [16] and connective tissues [17].

The morphology of the prepared scaffolds and the mean fiber diameters can be adjusted by varying the PLGA concentration in the electrospinning solutions. There are a number of publications describing the dependence of the morphological, mechanical and biological properties of electrospun PLGA scaffolds [18,19] and scaffolds prepared from other polymers [20,21] on the concentration of the polymer in the electrospinning solution. In such works [18,20], the dependence of the polymer concentration in electrospinning solutions on the morphological properties and fiber diameter of polymer scaffolds has been well described. However, the morphology analysis in such studies is limited to scanning electron microscopy (SEM) and porosity determination, omitting the fact that atomic force microscopy (AFM) can also be used to evaluate the morphology of scaffolds and individual fibers, as well as their surface roughness. In addition, there are contradictory results of the effect of polymer concentration on the mechanical [21,22] and biological properties [19,23] of electrospun scaffolds. For example, in reference [19], it is reported that increasing the polymer solution concentration allows an increase in the fiber diameter of the electrospun scaffolds, leading to an increase in cell proliferation and differentiation, while in reference [23], increasing the polymer concentration and fiber diameter does not change the cell proliferation rate on the scaffolds. In reference [23], it is shown that the mechanical properties (tensile strength, Young's modulus) of electrospun scaffolds decrease with increasing polymer concentration and fiber diameter, while in reference [21], it is demonstrated that the tensile strength and strain at break of the electrospun scaffolds increase with increasing electrospinning solution concentration and fiber diameter. There are also a few studies in which a scaffold with optimal morphology, mechanical and biological properties is selected among the fabricated scaffolds. This work is therefore focused on investigating the dependence of the PLGA electrospinning solution concentration on the resulting scaffold morphology (including morphology investigations via AFM), mechanical characteristics, degradation and biological properties of prepared scaffolds, in order to select PLGA samples with the most applicable properties for tissue engineering applications.

2. Materials and Methods

2.1. Scaffold Fabrication

PLGA granules (85/15, Corbion Purac, Amsterdam, The Netherlands), with the molecular weight of $M_n \approx 202,000$ g/mol and $M_w \approx 338,000$ g/mol and inherent viscosity in the range of 2.0–2.5 dL/g (measured at a room temperature of 25 °C, concentration 0.1 g/dL in chloroform (Ekos-1, Moscow, Russia)), were dissolved in hexafluoroisopropanol (HFIP, $(CF_3)_2CHOH$, P&M Invest, Moscow, Russia) to obtain polymer solutions. The concentrations of the prepared PLGA solutions were 2 wt.%, 3 wt.%, 4 wt.% and 5 wt.%. Subsequently, the obtained solutions were utilized to fabricate PLGA scaffolds through electrospinning employing a NANON-01A electrospinning system (MECC Co., Fukuoka, Japan). For

the scaffold preparation, the NANON-01A has been equipped with a grounded rotatable cylindrical collector (dimensions: 100 mm diameter, 200 mm length). A needle (gauge 20, internal diameter: 0.603 mm) with a length of 1 inch (25.4 mm) was attached to the syringe. The utilized voltage was +22 kV, the distance between the collector and the needle was 150 mm, the electrospinning solution flow rate was 4 mL/h, the rotational speed of the collector was 50 rpm and the spinneret speed was 10 mm/min. These electrospinning parameters were applied to all four PLGA electrospinning solutions. Subsequently, the fabricated electrospun PLGA scaffolds were placed in a vacuum chamber (Actan Vacuum, VTSH-K24-250-P, Moscow, Russia) at room temperature and a pressure of 100 Pa for 24 h. The PLGA scaffold samples are named below according to the electrospinning concentration used for fabrication: 2 wt.% PLGA electrospinning solution—2% PLGA scaffold, 3 wt.% PLGA electrospinning solution—3% PLGA scaffold, 4 wt.% PLGA electrospinning solution—4% PLGA scaffold, and 5 wt.% PLGA electrospinning solution—5% PLGA scaffold.

2.2. Viscosity

To measure the dynamic viscosity of the electrospinning solutions (PLGA in HFIP), an SV-10 viscometer (AND, Tokyo, Japan) was used. During the viscosity measurements, the temperature was $(21 \pm 3)^\circ\text{C}$.

2.3. Scanning Electron Microscopy—Scaffold Morphology

A scanning electron microscope (SEM, JCM-6000 Plus instrument, Jeol, Akishima, Japan) was used to obtain microscopic images of the surfaces of the PLGA scaffold samples. An accelerating voltage of 15 kV was used and the SEM micrographs were taken at magnifications of $1000\times$ and $5000\times$. Prior to SEM sample imaging, a sputter coater (SmartCoater, Jeol, Akishima, Japan) was used to enhance the electrical conductivity of the PLGA scaffolds by depositing a gold layer with a thickness of up to 100 nm. Fiber diameters were evaluated from SEM micrographs at $1000\times$ magnification with the software Fiji/ImageJ version 1.53v (National Institute of Health, Bethesda, MD, USA) [24,25], applied with the DiameterJ v1.018 plug-in (<https://imagej.net/plugins/diameterj>, accessed on 11 November 2022) [26].

2.4. Surface Roughness

Atomic force microscopy (AFM, NTEGRA NT-MDT AFM system, NT-MDT Spectrum Instruments, Moscow, Russia) was applied to determine the morphology and root mean square roughness (RMS) for scan areas of $40 \times 40 \mu\text{m}^2$, 1.0×1.0 and $0.5 \times 0.5 \mu\text{m}^2$. All PLGA scaffolds were scanned using NSG01 monocrystalline silicon cantilevers (NTEGRA NT-MDT AFM system, NT-MDT Spectrum Instruments, Moscow, Russia) with a force constant ranging from 1.45 to 15.10 N/m. Four to six AFM micrographs were scanned for each PLGA sample and for each scan area (for $40 \times 40 \mu\text{m}^2$ and for 1.0×1.0 , $0.5 \times 0.5 \mu\text{m}^2$). Subsequently, the root mean square (RMS) of the roughness R_{RMS} was calculated according to Equation (1) [27]:

$$R_{RMS} = \sqrt{\frac{1}{M \times N} \sum_{j=1}^M \sum_{i=1}^N (h_{i,j} - \bar{h})^2}, \quad (1)$$

where $M \times N$ is the dimension of the matrix containing the measured height data $h_{i,j}$, and \bar{h} is the mean height value calculated as the sum of all measured heights $h_{i,j}$, divided by the size of the matrix $M \times N$. All R_{RMS} values were calculated using Gwyddion 2.63 (Czech Metrology Institute, Jihlava, Czechia) [28].

2.5. Scaffold Porosity

The porosity values (P) of the fabricated scaffolds were obtained by the gravimetric method and calculated using Equation (2) [29]:

$$P = \left(1 - \frac{\rho_{scaffold}}{\rho_{solid}}\right) \cdot 100\%, \quad (2)$$

with $\rho_{scaffold}$ —the density of a PLGA scaffold in g/cm^3 , ρ_{solid} —the density of the copolymer PLGA ($1.25 \text{ g}/\text{cm}^3$) [30].

2.6. Raman Spectroscopy

Raman spectra of the prepared PLGA scaffolds were obtained using a Raman spectrometer (NTEGRA NT-MDT AFM-Raman system, NT-MDT Spectrum Instruments, Moscow, Russia) integrated into an atomic force microscope (AFM, NTEGRA NT-MDT AFM system, NT-MDT Spectrum Instruments, Moscow, Russia). The spectra were obtained at $100\times$ magnification by scanning the sample surfaces with a 532-nm laser in the green light region.

2.7. X-ray Crystallography

The crystalline structure of the PLGA scaffolds was investigated via X-ray diffraction (XRD) using an XRD 6000 X-ray diffractometer (Shimadzu, Kyoto, Japan). During the analysis, the following technological parameters were used: Cu-K α radiation— $\lambda = 1.54 \text{ \AA}$; X-ray tube voltage—40 kV; X-ray beam current—30 mA; scanning angle range— $10\text{--}80^\circ$; scanning speed— $2^\circ/\text{min}$; scanning step— 0.02° .

2.8. Sample Surface Wettability

A drop-shaped analyzer DSA-20 (Krüss, Hamburg, Germany) was employed to acquire water contact angles (WCA) and to take micrographs of water droplets after 2 s and after 1 min of their interaction with the surface of the PLGA scaffold samples. For each sample with an area of $3 \times 1 \text{ cm}^2$, three water droplets with a volume of $2 \mu\text{L}$ were dropped.

2.9. Mechanical Properties

The mechanical properties of the prepared PLGA scaffolds were evaluated using an Instron 3343 tensile tester (Illinois Tool Works, Glenview, IL, USA) equipped with an Instron 2519-102 static load cell of 50 N (Illinois Tool Works, Glenview, IL, USA). Traverse speed and area of the samples between the traverse jaws was $10 \text{ mm}/\text{min}$ and $10 \times 10 \text{ mm}^2$, respectively. Three PLGA scaffold samples of each type were used for the mechanical tests.

2.10. In Vitro Scaffold Degradation

Degradation test were performed according to the ISO 10993-13:2010 standard [31]. PLGA scaffolds with a sample area of $2 \times 2 \text{ cm}^2$ were placed in 2.5 mL Eppendorf tubes filled with phosphate-buffered saline (PBS) with a pH of 7.3–7.5 (Rosmedbio, St. Petersburg, Russia). The mass of the PLGA samples was measured before immersion in PBS and ranged from 5 to 20 mg, while the height of the samples varied from 60 to 150 μm . After immersion, the tubes were placed in an incubation chamber (ITM, ITM.SHS, Tomsk, Russia) at 37°C . The PBS solutions in the Eppendorf tubes were exchanged for new solutions every two weeks. After 1, 2 or 3 months, the PLGA samples were removed from the tubes and air-dried for 2 h. Thereafter, the residual water in the samples was removed in a vacuum chamber (Actan Vacuum, VTSH-K24-250-P, Moscow, Russia) at room temperature and a pressure of 100 Pa for 24 h.

After drying, the relative remaining dry mass ($M\%$) of the samples was estimated using Equation (3) [32]:

$$M\% = \frac{M_{dry}}{M_0} \times 100, \quad (3)$$

with M_0 being the initial mass of the sample before the degradation process, and M_{dry} is the mass of the completely dried scaffold sample that was placed in PBS solution for 1, 2 or 3 months.

The surface morphology of PLGA samples immersed in PBS solution for 1, 2 or 3 months was evaluated using an SEM (for more details see Section 2.3). SEM micrographs were obtained at a magnification of $1000\times$ and $5000\times$ as well as an accelerating voltage of 15 kV. Prior to SEM analysis, PLGA samples were coated with gold to enhance electrical conductivity (for more details see Section 2.3). Histograms of the fiber diameters were evaluated as described in Section 2.3. Three samples of each type were used for this experiment.

The molecular weight distributions (number average molecular weight (M_n) and molecular weight (M_w)) of the PLGA scaffold samples before degradation and after degradation at 1, 2 or 3 months were analyzed by gel permeation chromatography (GPC) using a liquid chromatograph (Agilent 1200 Infinity Agilent Technologies, Santa Clara, CA, USA) equipped with a PLgel 5 μm MIXED-C column (Agilent Technologies, Santa Clara, CA, USA). For this purpose, all scaffold samples were dissolved in chloroform (Ekos-1, Moscow, Russia) at 0.8% w/w and filtered through a 0.45 μm syringe filter before elution. Polystyrene was used as the standard for calibration, and chloroform was used as the eluent at a flow rate of 1 mL/min.

The differences in the molecular weight distributions (ΔM_n and ΔM_w) were calculated via Equations (4) and (5):

$$\Delta M_n = \Delta M_{ni} - \Delta M_{no}, \quad (4)$$

where ΔM_{ni} is the difference of M_n of the PLGA scaffolds immersed in PBS solution for 1, 2 and 3 months in PBS, and ΔM_{no} is the difference of M_n of PLGA scaffolds not immersed in PBS (Before PBS).

$$\Delta M_w = \Delta M_{wi} - \Delta M_{wo}, \quad (5)$$

where ΔM_{wi} is the difference of M_w of the PLGA scaffolds immersed in PBS solution for 1, 2 and 3 months in PBS, and ΔM_{wo} is the difference of M_w of PLGA scaffolds not immersed in PBS (Before PBS).

2.11. Cell Adhesion, Cytotoxicity and Biocompatibility

2.11.1. Cell Line Preparation

For these assays, embryonic mouse fibroblasts of the 3T3-L1 cell line were used as a biological test model. This cell type was chosen because the cells have a fibroblast-like morphology and can thus be utilized to regenerate soft tissue on the surface of porous non-woven scaffolds [33,34]. Cells were grown in Dulbecco's modified eagle medium (DMEM, Gibco, Billings, MT, USA) enriched with 2 mM glutamine (PanEco Ltd., Moscow, Russia), 10% fetal bovine serum (One Shot™, Thermo Fisher Scientific, São Paulo, Brazil) and antibiotics (50 IU/mL penicillin and 50 $\mu\text{g}/\text{mL}$ streptomycin, PanEco Ltd., Moscow, Russia). Cultivation was carried out under standard conditions in a CO_2 incubator (CB-170, Binder, Tuttlingen, Germany) with 5% carbon dioxide at 37 °C and 100% humidity. The cells were thus brought into the stable growth phase and used for the experiments.

2.11.2. Sample Treatment

The scaffolds investigated were PLGA scaffolds in the form of discs with a diameter of 10 mm. All discs were pre-sterilized in 99% ethanol (Rosbio, St. Petersburg, Russia) for 2 h and dried in a vacuum oven (Actan Vacuum, VTSH-K24-250-P, Moscow, Russia) at room temperature and 100 Pa for 24 h. All polymer discs were kept in sterile 24-well plates (SPL Life Sciences Co., Ltd., Pocheon, Republic of Korea) completely filled with 1 mL DMEM medium (the same as used for cell cultivation) for 5 days to solubilize potentially toxic polymer components from the scaffold samples. Daily visual inspection was performed on all samples. The DMEM medium with a volume of 1 mL per well without a sample disc was used as control. After 5 days of extraction of the toxic polymer components, the

DMEM medium solutions were collected and analyzed for cytotoxicity and cell growth by cell morphology (via fluorescence microscopy) and standard cell viability assay (see below, Section 2.11.3).

2.11.3. Cell Viability Tests

To evaluate the cytotoxic effects of the polymer extracts, 3000 fibroblasts (counted with an automated cell counter (Countess 2FL, Thermo Fisher Scientific Inc., Waltham, MA, USA)) per well were seeded into the wells of a sterile 96-well plate (SPL Life Sciences Co., Ltd., Pocheon, Republic of Korea) at 24 h before the start of the tests. After 24 h, the medium in the wells was replaced with the 5-day DMEM medium extracts from the samples (preparation is described above in Section 2.11.2). All plates were then placed in an incubator (CB-170, Binder, Tuttlingen, Germany) and cultured under standard conditions at 37 °C and 5% CO₂. Cell viability was assessed after 1, 3 and 5 days using MTT assays. For this purpose, the DMEM medium in the well plate was replaced with a solution of 3-(4,5-dimethylthiazol-2-yl)-2,5-diphenyl-2H-tetrazolium bromide (MTT, PanEco Ltd., Moscow, Russia) at a concentration of 0.45 mg/mL and the well plate was placed in a CO₂ incubator (CB-170, Binder, Tuttlingen, Germany) at 37 °C for 4 h. Thereafter, the MTT solution was removed and dimethyl sulfoxide (DMSO, PanEco Ltd., Moscow, Russia) was added to dissolve the formed formazan in a volume of 100 µL. The optical density of the samples was then measured at a wavelength of 570 nm employing a microplate photometer (Multiskan FC, Thermo Fisher Scientific Inc., Waltham, MA, USA). All optical density values measured were processed and the viability was calculated as a percentage of the control group.

The cell viability (V) was calculated according to Equation (4) [35]:

$$V = \frac{OD_{scaffold}}{OD_{control}} \times 100\%, \quad (6)$$

where $OD_{scaffold}$ is the optical density of cells on PLGA scaffolds, and $OD_{control}$ is the optical density of cells on control samples.

2.11.4. Biocompatibility Testing

To assess the biocompatibility, the polymer discs were placed on the bottom of a 24-well plate (SPL Life Sciences Co., Ltd., Pocheon, Republic of Korea) and seeded with a fibroblast cell suspension at a concentration of 5×10^4 cells/mL. The monitoring of cell growth and assessment of cell density on the surface of the sample discs was performed after 1, 3 and 5 days by staining with fluorescent dyes (according to the protocol in the paragraph below). Fluorescent micrographs were taken using an inverted microscope (Zeiss AxioVert A1, Carl Zeiss AG, Oberkochen, Germany) and subsequent counting of cells was performed using ImageJ software 1.53v (for more details see Section 2.3). For each sample, at least 4 micrographs were taken at 100× magnification. The surface area of the micrographs was 1.278 mm². After counting the cells of all micrographs, the mean values were calculated as the number of cells per 1.0 mm² of the surface of the corresponding sample. The cell density ratio (CDR) was calculated as the ratio of the cell density on the PLGA scaffolds discs ($NC_{scaffold}$) to the cell density on the control samples ($NC_{control}$) [35]:

$$CDR = \frac{NC_{scaffold}}{NC_{control}} \times 100\%. \quad (7)$$

2.11.5. Cell Morphology, Cell Growth and Cell Viability

The morphology, growth, and viability of cells on the surface of the PLGA scaffold discs were investigated by fluorescence imaging using a Zeiss AxioVert A1 inverted microscope (Carl Zeiss AG, Oberkochen, Germany). A mixture of the vital fluorescent dyes Calcein AM (0.5 µg/mL) and Hoechst 33342 (1 µg/mL) in a volume of 200 µL was added to each scaffold sample disc with cells growing on its surface. Samples were kept in a CO₂ incubator CB-170 (Binder, Tuttlingen, Germany) at 37 °C for 15 min, and then a microscopic

examination was carried out. Images were obtained using ZEN pro 2.3 software (Carl Zeiss AG, Oberkochen, Germany).

The schematic overview of the fabrication of PLGA scaffolds by electrospinning and the further applied investigation methods are shown in Figure 1.

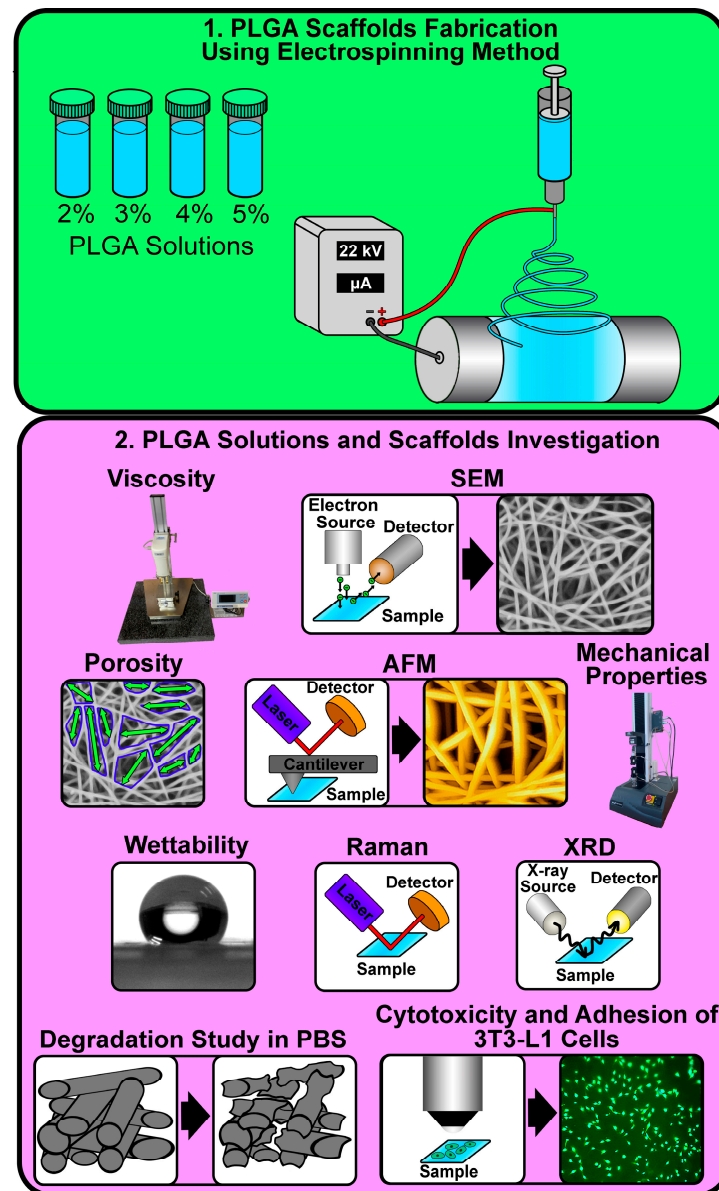


Figure 1. Schematic illustration of the preparation of poly(lactide-co-glycolide) (PLGA) scaffolds and their further investigation. In the first stage, PLGA scaffolds were formed by electrospinning from electrospinning solutions with PLGA concentrations of 2, 3, 4, and 5 wt.%. The second section of this figure provides an overview of all the investigation methods performed in this study.

3. Results

3.1. Dynamic Viscosity of the Electrospinning Solutions

As the concentration of poly(lactic-co-glycolic acid) (PLGA) in the electrospinning solution increased, the dynamic viscosity also increased. The viscosities of the 2, 3, 4 and 5 wt.% electrospinning solutions were 169 ± 10 , 336 ± 18 , 745 ± 18 , and 877 ± 35 mPa \times s, respectively (Supplementary Information (SI) Figure S1).

3.2. Surface Morphology and Porosity of the Scaffolds

Scanning electron microscopy (SEM) micrographs taken at 1000 \times and 5000 \times magnifications and atomic force microscopy (AFM) images micrographs taken at scanning areas of 40 \times 40 μm^2 , 1.0 \times 1.0 μm^2 and 0.5 \times 0.5 μm^2 of the 2, 3, 4, and 5 wt.% PLGA scaffold samples are shown in Figure 2.

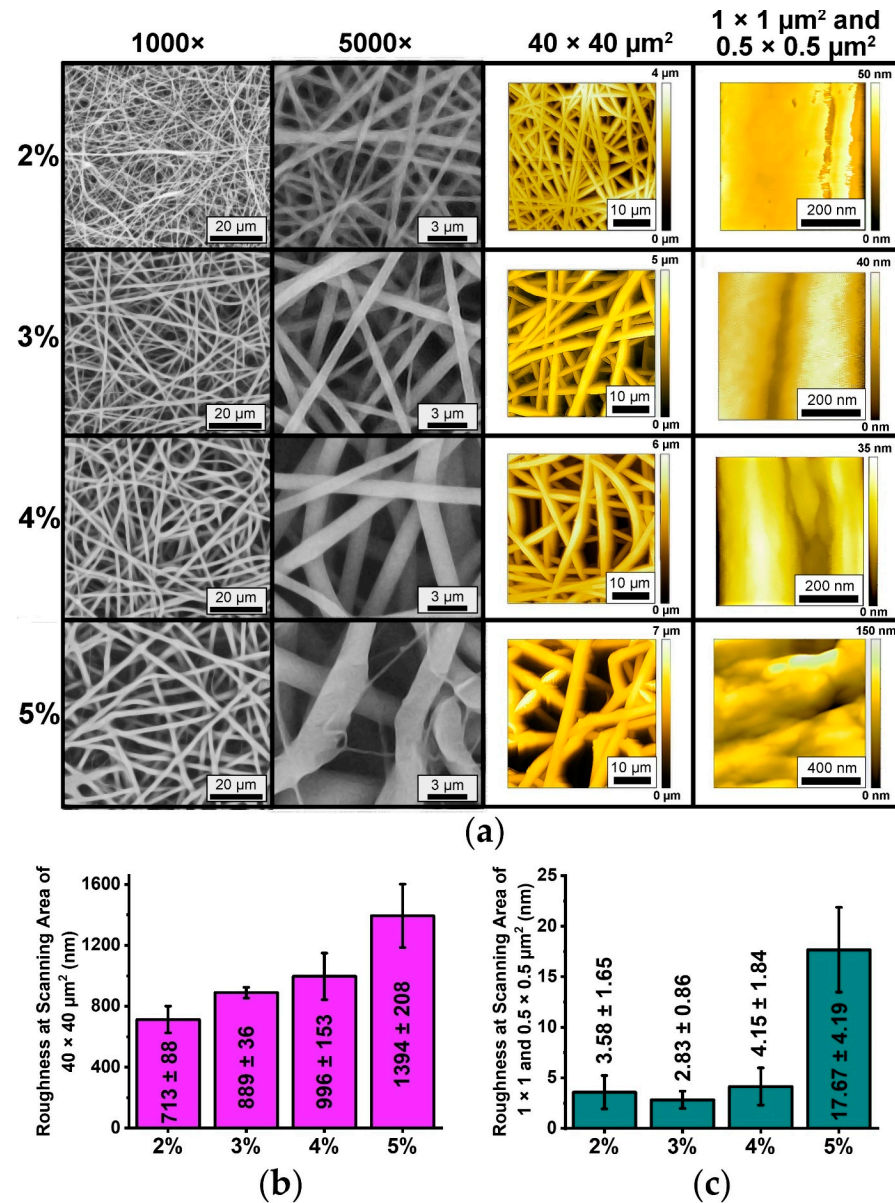


Figure 2. (a) SEM micrographs at 1000 \times (first column) and 5000 \times (second column) magnification and AFM micrographs taken at scanning areas of 40 \times 40 μm^2 (third column), 1.0 \times 1.0 μm^2 and 0.5 \times 0.5 μm^2 (fourth column) of poly(lactide-co-glycolide) (PLGA) scaffolds fabricated from electrospinning solutions containing different concentrations of PLGA (2, 3, 4, 5 wt.%), as well as the roughness of PLGA scaffolds prepared from electrospinning solutions with different PLGA concentrations (2, 3, 4 and 5 wt.%) dissolved in hexafluoro-2-propanol (HFIP). The roughness has been measured by atomic force microscopy (AFM): (b) roughness determined at a scanning area of 40 \times 40 μm^2 and (c) roughness measured at scanning areas of 1.0 \times 1.0 μm^2 and 0.5 \times 0.5 μm^2 .

From the SEM micrographs, it can be observed that the morphology of the PLGA scaffolds exhibited intertwined fibers (Figure 2a, first and second columns). As the PLGA concentration in the electrospinning solutions increased from 2 to 5 wt.%, the

fiber diameter of the electrospun scaffolds also increased. For the PLGA scaffold samples, the fiber diameters immediately after fabrication were $0.79 \pm 0.33 \mu\text{m}$ —2% PLGA scaffolds, $1.05 \pm 0.38 \mu\text{m}$ —3% PLGA scaffolds, $1.36 \pm 0.46 \mu\text{m}$ —4% PLGA scaffolds, and $1.79 \pm 0.73 \mu\text{m}$ —5% PLGA scaffolds (Figure 3, Before PBS). In the case of the 5% PLGA scaffold samples, a few nanofibers with a size of 200–300 nm could be observed at $5000\times$ magnification, in addition to microfibers (Figure 2a, second column).

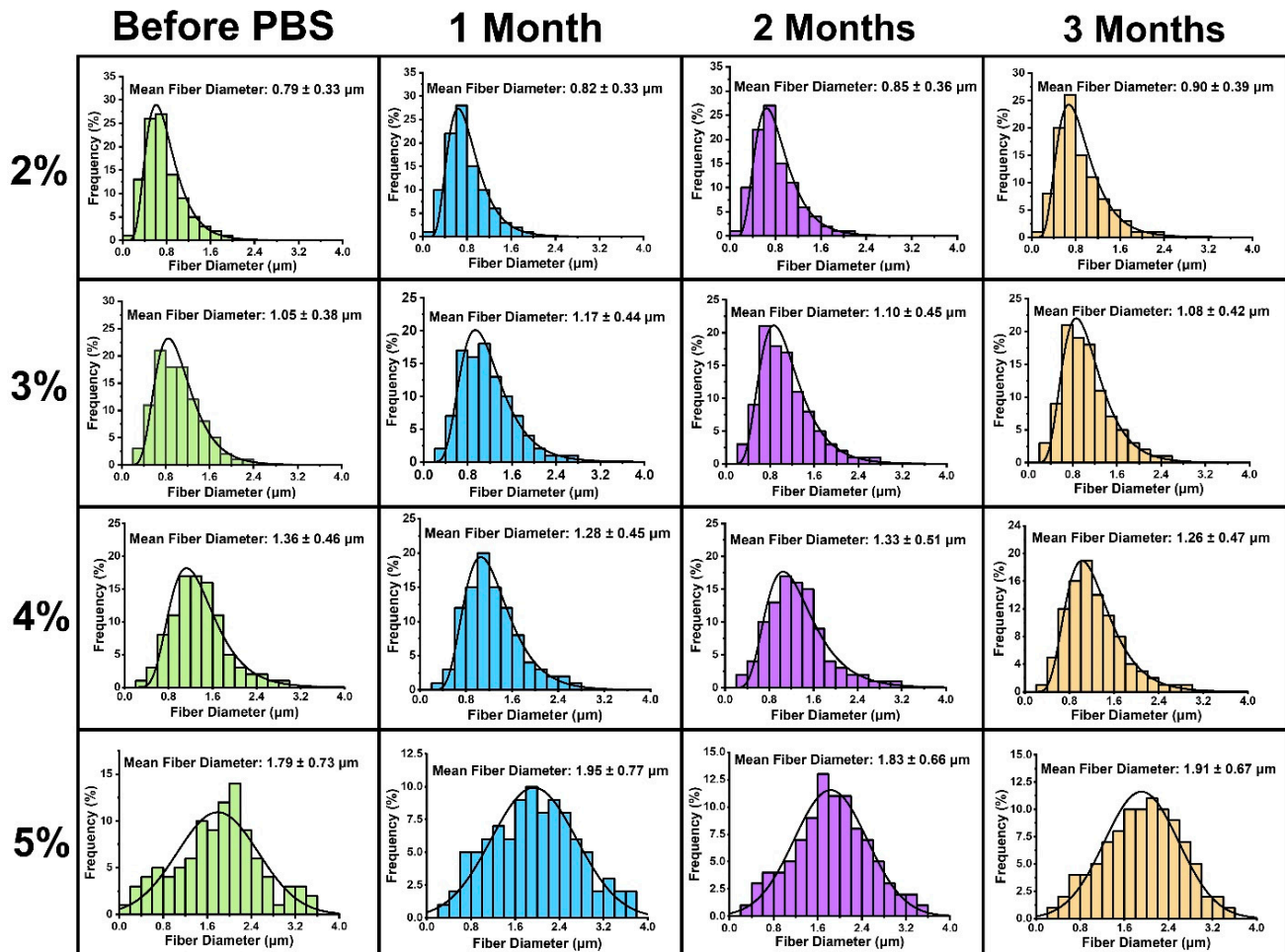


Figure 3. Mean fiber diameters (bars in the corresponding color) and histograms (distribution line in black) assessed from scanning electron microscopy (SEM) micrographs at $1000\times$ magnification of poly(lactide-co-glycolide) (PLGA) scaffolds not immersed (Before PBS, olive) and immersed in phosphate-buffered saline (PBS) for 1 (light blue), 2 (purple) or 3 months (beige) and fabricated from solutions with different concentration (2, 3, 4 and 5 wt.%) of PLGA dissolved in hexafluoro-2-propanol (HFIP).

As evident from the SEM micrographs, a fibrous structure on the PLGA scaffolds can also be seen on the AFM micrographs with a scanning area of $40 \times 40 \mu\text{m}^2$ (Figure 2a, third column). The roughness values of the PLGA scaffolds at a scanned area of $40 \times 40 \mu\text{m}^2$ were $713 \pm 88 \text{ nm}$ —2% PLGA scaffolds, $889 \pm 36 \text{ nm}$ —3% PLGA scaffolds, $996 \pm 153 \text{ nm}$ —4% PLGA scaffolds, and $1394 \pm 208 \text{ nm}$ —5% PLGA scaffolds (Figure 2b). As the PLGA concentration in the electrospinning solutions increased, the roughness of the fabricated PLGA scaffolds also increased for the values obtained at a scanning area of $40 \times 40 \mu\text{m}^2$. The surfaces of individual PLGA fibers are represented in the AFM micrographs obtained in scanning areas of $1.0 \times 1.0 \mu\text{m}^2$ and $0.5 \times 0.5 \mu\text{m}^2$ (Figure 2a, fourth column). For the PLGA scaffold fibers, the surface roughness of individual fibers did not differ significantly: $3.58 \pm 1.65 \text{ nm}$ for 2% PLGA scaffolds, $2.83 \pm 0.86 \text{ nm}$ for 3% PLGA scaffolds, and $4.15 \pm 1.84 \text{ nm}$ for 4% PLGA scaffolds (Figure 2c). For 5% PLGA scaffolds, the surface roughness of the fibers was

17.67 ± 4.19 nm, which is 4–6 times higher than the roughness for the 2%, 3%, and 4% PLGA scaffolds (Figure 2c).

The porosity values measured by the gravimetric method (see Section 2.5 for more details) for the samples were $85\% \pm 3\%$ for 2% PLGA scaffolds, $82\% \pm 4\%$ for 3% PLGA scaffolds, $80\% \pm 5\%$ for 4% PLGA scaffolds, and $74\% \pm 5\%$ for 5% PLGA scaffolds (SI Figure S2).

3.3. Raman Spectroscopy and X-ray Diffraction

In each Raman spectrum of all scaffold samples investigated, the three most intense peaks can be observed at Raman shifts of 877 cm^{-1} , 1458 cm^{-1} , and 1775 cm^{-1} (SI Figure S3). No significant changes in the Raman spectra were observed with increasing PLGA concentrations in the electrospinning solution. From the Raman spectra, it can be concluded that the PLGA scaffolds prepared were of high purity and had no solvent residues.

The X-ray diffraction method (XRD) was used to demonstrate the amorphous structure of all PLGA scaffolds studied, as evidenced by the presence of broad halos in the range of 10° – 30° on all diffractograms (SI Figure S4).

3.4. Wettability and Mechanical Properties

The water contact angles (WCA) of the PLGA scaffolds ranged from 126° to $129^\circ \pm 3^\circ$ after 2 s of contact with the scaffold surfaces (Supplementary Material Figure S5, 2 s). After a one-minute interaction of the water droplets with the PLGA scaffold surfaces, the WCA values did not change significantly, and varied in the range of 125° – $129^\circ \pm 3^\circ$ (SI Figure S5, 1 min). As a result, the PLGA scaffolds prepared from electrospinning solutions with different PLGA concentrations showed almost identical WCA values with different morphologies. In addition, the water droplets on the surface of PLGA scaffolds were stable and their WCA did not change with up to 1 min of interaction with the samples.

The mechanical properties of the prepared PLGA scaffolds increased with increasing PLGA concentrations (from 2 wt.% to 5 wt.%) in the electrospinning solutions (SI Figure S6). The measurement results of the mechanical properties show that the PLGA scaffolds had the following tensile strength values: 4.0 ± 0.6 MPa for the 2% PLGA scaffolds, 4.7 ± 0.2 MPa for the 3% PLGA scaffolds, 5.5 ± 0.3 MPa for the 4% PLGA scaffolds, and 5.6 ± 0.3 MPa for the 5% PLGA scaffolds (SI Figure S6a). The maximum elongation values for the PLGA scaffolds were as follows: $161\% \pm 17\%$ for the 2% PLGA scaffolds, $244\% \pm 19\%$ for the 3% PLGA scaffolds, $353\% \pm 15\%$ for the 4% PLGA scaffolds and $501\% \pm 24\%$ for the 5% PLGA scaffolds (SI Figure S6b).

3.5. In Vitro Degradation Study

For all PLGA scaffolds, the remaining masses were in the range of 98 – $103\% \pm 5\%$ after being immersed in phosphate-buffered saline (PBS) for 1, 2 or 3 months to assess hydrolytic degradation (SI Figure S7). This indicates that all PLGA samples did not significantly change their mass after immersion in PBS.

The molecular weights of the PLGA scaffolds were in the range of $(1.88$ – $2.22) \times 10^5$ g/mol for the number average molecular weight (M_n) and $(3.38$ – $3.89) \times 10^5$ g/mol for the molecular weight (M_w), respectively (SI Figure S8a,b). The average molecular weight difference (ΔM_n) values were in the range of $(-0.14$ – $0.20) \times 10^5$ g/mol and the molecular weight differences (ΔM_w) were in the range of $(0.27$ – $0.51) \times 10^5$ g/mol (SI Figure S8c,d). These results indicate that the molecular weights of all PLGA scaffolds were not significantly different after hydrolytic degradation over 1, 2 or 3 months.

Mean fiber diameters and histograms evaluated from SEM micrographs at $1000\times$ magnification for all PLGA scaffold samples that were not immersed (Before PBS) and immersed in PBS for 1, 2 or 3 months are displayed in Figure 3.

The SEM micrographs of the PLGA scaffold samples after 1, 2 or 3 months in PBS show that the fibrous structure was retained in all samples (SI Figures S9 and S10). After

one month of immersion of PLGA scaffolds in PBS, the SEM micrographs at 1000 \times and 5000 \times magnification show that the fibers were intact, with no significant defects. After the first month of immersion in PBS, the mean fiber diameters of the PLGA scaffolds were as follows: $0.82 \pm 0.33 \mu\text{m}$ —2 wt.% PLGA scaffolds, $1.17 \pm 0.44 \mu\text{m}$ —3 wt.% PLGA scaffolds, $1.28 \pm 0.45 \mu\text{m}$ —4 wt.% PLGA scaffolds, and $1.95 \pm 0.77 \mu\text{m}$ —5 wt.% PLGA scaffolds (Figure 3, 1 month). These values for the fiber diameters were not significantly different from the values for the PLGA scaffolds that were not immersed in PBS (Figure 3, Before PBS). This indicates that all PLGA scaffold samples showed no significant changes in morphology after 1 month in PBS.

After the PLGA scaffolds were immersed in PBS for 2 months, it can be observed that the morphologies did not change again significantly (SI Figures S9 and S10, 2 months). The fiber diameters of the PLGA scaffolds after 2 months in PBS were $0.85 \pm 0.36 \mu\text{m}$ —2 wt.% PLGA scaffolds, $1.10 \pm 0.45 \mu\text{m}$ —3 wt.% PLGA scaffolds, $1.33 \pm 0.51 \mu\text{m}$ —4 wt.% PLGA scaffolds, and $1.83 \pm 0.66 \mu\text{m}$ —5 wt.% PLGA scaffolds (Figure 3, 2 months). These results are again not significantly different from the mean fiber diameters of the PLGA scaffolds that were not immersed in PBS (Figure 3, Before PBS).

Finally, no significant changes in the scaffold surface morphologies were observed after 3 months. This conclusion is confirmed by the PLGA scaffolds mean fiber diameter values evaluated, which are as follows: $0.90 \pm 0.39 \mu\text{m}$ for the 2 wt.% PLGA scaffolds, $1.08 \pm 0.42 \mu\text{m}$ for the 3 wt.% PLGA scaffolds, $1.26 \pm 0.47 \mu\text{m}$ for the 4 wt.% PLGA scaffolds, and $1.91 \pm 0.67 \mu\text{m}$ for the 5 wt.% PLGA scaffolds (Figure 3, 3 months). These values of fiber diameters are again not significantly different from the fiber diameters for the PLGA samples that were not immersed in PBS (Figure 3, Before PBS). However, at a magnification of 5000 \times (SI Figure S10, 3 months), it can be seen that some fibers of the PLGA scaffolds appeared broken after 3 months in PBS.

As a result, it can be seen that there were no significant changes in the morphology and mean fiber diameter of the PLGA scaffold samples after being immersed in PBS for 1, 2, or 3 months.

3.6. Biological Properties

Optical fluorescence microscope images of mouse 3T3-L1 embryonic fibroblasts on PLGA scaffolds are presented in Figure 4.

The morphology of mouse 3T3-L1 embryonic fibroblasts on the PLGA scaffold samples can be observed on fluorescence micrographs (Figure 4). Cells were evenly distributed on the surfaces of all PLGA scaffolds, and no dead cells were observed. On the fifth day of incubation, a visual change in the color of the medium was observed on all samples, indicating an acidification process (Figure 4, Day 5). With an increase in the incubation time from 1 to 5 days, an increase in the amount of the cells was observed on all PLGA scaffolds. The cells were viable on all PLGA samples and displayed no visible differences between them. It should be noted that the morphological parameters of the cell cultures are comparable to those of the control group (medium without PLGA samples). This indicates a normal state of cell growth and cell division.

The assay results of cell adhesion, cell proliferative activities, and cytotoxicity of the 3T3-L1 cells on the PLGA scaffolds are shown in Figure 5.

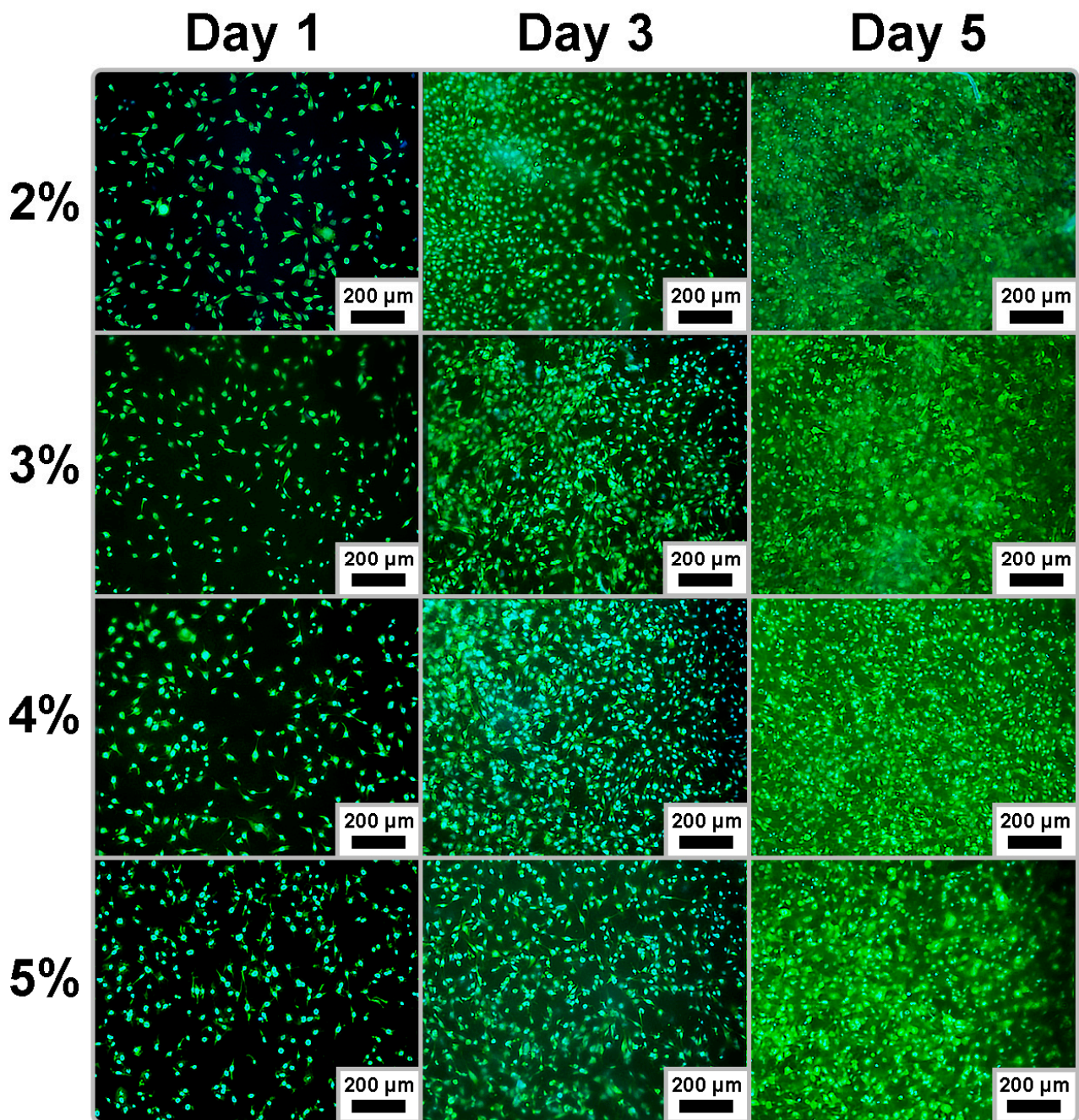


Figure 4. Fluorescence micrographs of 3T3-L1 cells on PLGA scaffolds at 100× magnification on the first, third and fifth days of cell incubation. The PLGA scaffold was prepared from electrospinning solutions containing different concentrations of PLGA (2, 3, 4, and 5 wt.%).

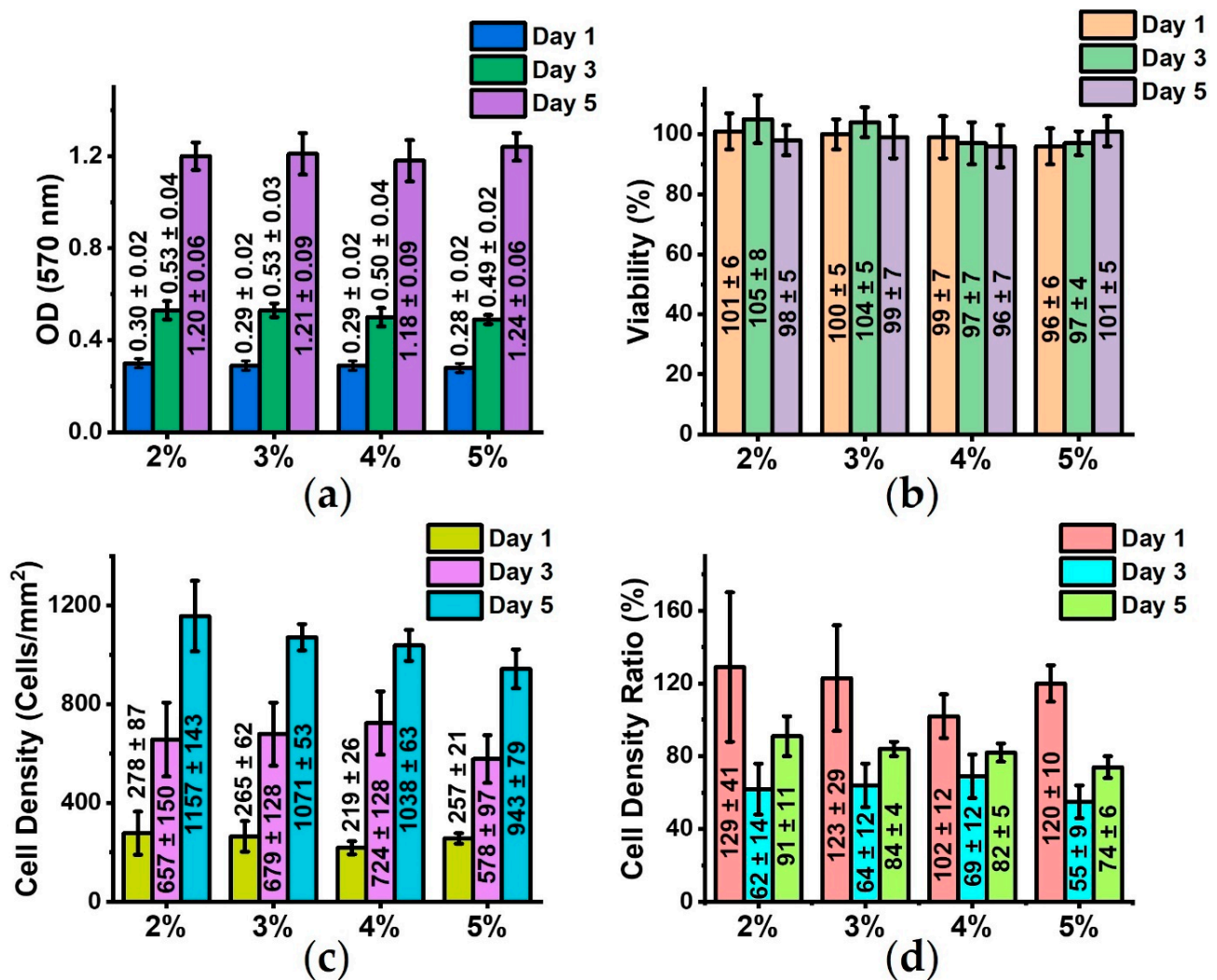


Figure 5. Assay results of cell cultivation and cytotoxicity with mouse 3T3-L1 embryonic fibroblasts: (a) Cell proliferative activity as optical density at 570 nm with PLGA scaffold sample extracts; (b) cytotoxicity assay as cell viability in percent for the investigated PLGA scaffold extracts; (c) cell densities of 3T3-L1 cells on the PLGA scaffolds determined from optical fluorescence micrographs (see Figure 4); (d) cell density ratio in percent calculated according to Equation (5) (Section 2.11.4).

The cytotoxicity, cell proliferative activity (via optical density) and cell adhesion studies showed that all PLGA scaffolds exhibited no toxic properties toward the mouse 3T3-L1 embryonic fibroblasts (Figures 4 and 5).

Within 5 days, the optical density values increased by 4.0–4.5 times for all PLGA scaffold extracts (Figure 5a). This indicates that the PLGA samples did not contain or release toxic compounds, and thus normal cell growth and cell division occurred. When examining the relative cell viabilities calculated from the optical densities, it can be observed that the normalized viability for all PLGA samples ranged from 97 to 105% ± 8% (Figure 5b). These values indicate that the cell densities of the PLGA samples extracts were not significantly different from those of the control samples. The cell densities assessed from fluorescence micrographs of 3T3-L1 fibroblasts on PLGA scaffolds (Figure 4) show that the cell densities increased from day 1 to 5, from 257–278 cells/mm² ± 87 cells/mm² to 943–1157 cells/mm² ± 143 cells/mm² (Figure 5c), indicating a 3.4–4.5-fold increase in cell quantity. On days 1 and 3, the numbers of cells were not significantly different for all PLGA samples (Figure 5c). However, on day 5, the number of cells on the surface of the scaffolds decreased slightly with increasing PLGA concentration (Figure 5c). On day 5, when the

PLGA concentration in the electrospinning solutions increased by 1%, the number of cells on the corresponding PLGA scaffolds decreased by 3% to 10% (Figure 5c). The highest cell density ratio was observed on day 1 (Figure 5d). Thus, 2–29% more cells were observed on the PLGA scaffolds than in the medium without PLGA scaffolds (control). The lowest cell density ratio was observed on day 3, since the number of cells on the PLGA scaffolds was 31% to 45% lower than in the control group. On day 5, the number of cells on PLGA scaffolds was 9% to 26% lower than in the control group (Figure 5d).

4. Discussion

The directly proportional dependence of the viscosity of the PLGA spinning solution on the polymer concentration (SI Figure S1) is in agreement with reference [36]. As the polymer concentration in the electrospinning solution increases, its viscosity increases because the number of polymer chains in the solution increases. At a low concentration, the polymer chains in the solution hardly interact with each other because they are dispersed in the solvent, but at a high concentration, the polymer chains may start to intertwine with each other [36], which increases the viscosity of the electrospinning solution. Chain entanglement in the electrospinning solution is the main factor for the successful formation of polymer fibers by electrospinning [36]. The overlapping and entanglement of polymer chains in the solution allows the formation of stable charged fluid jets during electrospinning [37]. Moreover, the degree of entanglement of the polymer chains in the electrospinning solution can be roughly estimated by measuring the viscosity of the electrospinning solution and considering the concentration of the polymer in solution [36]. However, it should be noted that electrospinning solutions that are too viscous can negatively affect the formation of the charged fluid jet and thus the phase separation during the electrospinning process due to their high surface tension [37].

A significant increase in fiber diameter with increasing polymer concentration in solution has been reported in the literature [21,38]. The increase in fiber diameter with an increasing concentration of PLGA in the electrospinning solution from 2 wt.% to 5 wt.% is associated with an increase in the viscosity of the respective electrospinning solutions, as a result of which the surface tension is able to more strongly resist the Coulomb force [39], which leads to the formation of electrospinning jets with larger diameters. Fiber diameter is an important characteristic for electrospun scaffolds because their biological properties depend on this parameter [40].

An increase in the roughness of the nonwoven PLGA scaffold surfaces with an increase in the concentration of the electrospinning solutions also indicated an increase in pore sizes. This results from Equation (1), for the calculation of the root mean square roughness R_{RMS} (Section 2.4). The increase in pore size is directly related to the increase in fiber diameter, thus a linear dependence of fiber diameters on the pore sizes of the electrospun scaffolds has been demonstrated in reference [41].

The high roughness of the 5 wt.% scaffolds indicates the pronounced relief of the individual fibers, and might be due to the fact that in some areas the fibers do not have the cylindrical form of the 2 wt.%, 3 wt.%, and 4 wt.% scaffolds, but are flattened, which can be seen from the SEM micrographs at 5000× magnification (Figure 2a, second column). In addition, the fibers in the nanometer diameter range of the 5 wt.% scaffolds also showed increased surface topography and roughness when stacked on fibers in the micrometer diameter range.

As the concentrations of the electrospinning solutions increased, the porosity of the prepared PLGA scaffolds decreased only insignificantly (SI Figure S2). These results are consistent with those reported in the literature [42], where smaller porosity values were observed for electrospun scaffolds with larger fiber diameters. Likewise, it is shown in reference [43] that increasing the polymer concentration in the electrospinning solution increases the resulting fiber diameter, while decreasing the porosity of the electrospun scaffolds. The porosity of electrospun scaffolds, resulting from the fiber diameter and

pore size, is an important parameter that can be used to predict the cellular activity of the scaffolds [44].

The position, shape and intensity of the peaks in the Raman spectra (SI Figure S3) indicate that all the samples investigated are scaffolds composed of the copolymer PLGA [45]. This fact is confirmed by the observation that the shape and intensity of the Raman spectra of the PLGA scaffolds did not change with increasing PLGA concentrations in the electrospinning solutions.

The halos obtained in the XRD diffractograms (SI Figure S4) are usually related to the copolymer PLGA [46]. The amorphous structure of PLGA scaffolds indicates that the polymer chains in the scaffold are irregularly arranged, and do not possess a long-range order. Depending on the stereochemistry, composition and molar ratio of glycolic acid and lactic acid, PLGA can be semi-crystalline or amorphous [47]. Amorphous copolymers are the result of disordered polymer chains [48], and the preparation of PLGA with a high degree of crystallinity is a complicated task because increasing the amount of glycolic acid in the copolymer increases the degree of racemization [49]. In drug delivery and other biomedical applications, amorphous PLGA is preferable to semi-crystalline PLGA because the active pharmaceutical agents and other biologically active compounds are more homogeneously distributed in amorphous PLGA [50,51]. Although the morphology of the scaffold changes significantly and the porosity decreases slightly, this does not affect the wettability of the scaffold. High WCA values (SI Figure S5) and thus hydrophobic properties are typical for electrospun PLGA scaffolds [52,53].

The observation that the mechanical properties of PLGA scaffolds improve with increasing PLGA concentration in the electrospinning solutions can be explained by the significant difference in morphology, since the polymer samples with the highest fiber thickness have the highest mechanical properties, while the scaffolds with the lowest fiber thickness have the lowest (Figure 3 and SI Figure S6). These results correlate with those in references [54,55], which reported that the mechanical properties (stiffness, tensile strength, elongation) depend linearly on the fiber thickness of electrospun scaffolds. Nevertheless, there are research articles in which the mechanical properties (tensile strength, elastic modulus) of electrospun scaffolds decrease with increasing fiber diameter [56,57]. Moreover, as the polymer concentration increases, the fiber diameter increases, but the mechanical properties may increase [21] or decrease [22]. This indicates that the dependence of mechanical properties of scaffolds on polymer concentration is complex, and that it is not always possible to predict the mechanical properties of scaffolds based on fiber size alone. Thus, in addition to the fiber size, the porosity of the scaffolds must also be determined, as it is also an important factor influencing the mechanical properties of the scaffolds. As porosity decreases, the compression strength [58], compression modulus [58,59] and elastic modulus [60] of the polymeric scaffolds decrease. Thus, the increase in mechanical properties with increasing PLGA concentration in the electrospinning solutions can be explained by the decrease in scaffold porosity. In the case studied here, less porous scaffolds have better mechanical properties due to their higher density, which can be derived from Equation (2) (Section 2.5). Electrospun scaffolds must have high mechanical properties to prevent their destruction under deformation forces, because when the mechanical integrity of the scaffolds is violated during deformation, the entire tissue engineering scaffold becomes unusable [22]. The mechanical properties of the electrospun scaffolds are an important factor determining their application in tissue engineering [22]. Depending on the mechanical properties of the PLGA scaffolds produced, they can be also effectively applied to regenerate skin tissue. In order to use scaffolds for skin regeneration, their mechanical properties should be similar to those of native skin, with a tensile strength of 5 MPa to 30 MPa and a relative elongation of 35% to 115% [61]. However, in reference [62], it has been reported that human skin can stretch up to 3.07 times. Therefore, the 4 wt.% PLGA scaffolds prepared in this study can be selected as the optimal samples in terms of mechanical properties, since their tensile strength is 5.5 ± 0.3 MPa and their maximum elongation at break is $353\% \pm 15\%$ (SI Figure S6), which are as close as possible to the values

reported in the literature [61,62]. Scaffold samples prepared with 2 wt.% and 3 wt.% of PLGA are not suitable because their tensile strength was below 5 MPa and their maximum elongation at break was less than 307%. In comparison, the scaffold samples prepared with 5 wt.% PLGA showed high tensile strength, but their maximum elongation at break significantly exceeded the value of 307%.

The hydrolytic degradation of PLGA can be divided into four steps: (1) the hydration step, in which water penetrates the copolymer and causes hydrogen bond cleavage between the polymer chains; (2) the initial degradation step, in which covalent bonds are broken, resulting in a decrease in molecular weight; (3) the constant degradation step, in which the covalent bonds are broken from the polymer backbone, leading to a decrease in the mass and a loss of its integrity; (4) the step of solubilization, in which individual polymer fragments are broken down into molecules that are subsequently dissolved in the surrounding aqueous medium [50]. In the case studied here, the degradation of PLGA scaffolds did not reach the second and the third steps because no significant changes in molecular weight and mass were observed for each of the PLGA samples, which were immersed in PBS for 1, 2 and 3 months (SI Figures S7 and S8).

The degradation rate of a PLGA scaffold slows down mainly with the increase in molecular weight [63] and with the increase in the ratio of the monomers lactic acid (LA) to glycolic acid (GA) (LA/GA) [64]. In reference [65], electrospun PLGA scaffolds (monomer ratio: LA:GA = 75:25, $M_w = 66,600$ – $107,000$ g/mol) lost 10% of their initial mass after 1 month and 14.8% after 2 months in PBS. For electrospun scaffolds of pure polylactic acid (PLA) with an extremely high molecular mass ($M_w = 450,000$ g/mol), the remaining mass of the scaffolds did not change over 45 days in PBS [66]. Also, in [67], it is shown that poly(L-lactic acid) with the highest molecular weight lost its molecular weight the slowest, over a period of 20 weeks. Regarding the study performed here, the retention of residual mass for all PLGA scaffolds in PBS for 3 months can be explained by the fact that the PLGA used had a high LA/GA monomer ratio (85/15) and an extremely high M_w (338,000 g/mol) (see Section 2.1). PLGA scaffolds with high molecular weight and amorphous structure could be excellent carriers for drug delivery and provide long-term release of one to six months [48]. The LA/GA monomer ratio used here (85/15) is very common for PLGA scaffolds and has been shown to be effective for the regeneration of nerves [68], bone [69,70] and soft tissue [71,72].

The absence of changes in morphology and mean fiber diameter after the immersion of PLGA samples in PBS for 1, 2, or 3 months (Figure 3, SI Figures S9 and S10) may be related to the retention of the initial mass (SI Figure S7) and initial molecular weight (SI Figure S8) of the copolymer PLGA and its monomer ratio (LA/GA). In reference [73], it is reported that the hydrolytic degradation of PCL/PLGA electrospun scaffolds (PCL— $M_w = 80,000$ and PLGA—LA/GA = 80/20, $M_w = 200,000$) is extremely slow, since no significant differences in morphology were observed in SEM micrographs after 150 days in PBS. Moreover, it is reported in reference [74] that the residual masses and SEM micrographs of electrospun scaffolds immersed in PBS for 3 months were similar to those of scaffolds not immersed in PBS.

All PLGA samples showed no toxicity towards 3T3-L1 fibroblasts (Figures 4 and 5). There are a number of studies showing that electrospun PLGA scaffolds have good biocompatibility with fibroblasts [18,75] and other cell types [16,76]. The decrease in the fibroblast density on PLGA scaffolds with increasing PLGA concentration in the electrospinning solutions (Figure 5c) might be related to the increase in fiber diameter and pore size, which promotes cell migration into the bulk volume of the scaffolds. Cell proliferation and migration on electrospun scaffolds with a mean fiber diameter less than $0.25 \mu\text{m}$ occurs mainly at the surface of the scaffolds, and as the fiber diameter increases, the cells will penetrate into the bulk volume of the scaffold [77]. This is due to the fact that as the fiber diameter increases, the pore size of electrospun scaffolds also increases [77], which promotes cell migration into the scaffold bulk volume. Hence, if the polymer concentration in the electrospinning solutions increases, the diameters of the fibers in the PLGA scaffolds

also increase, allowing the 3T3-L1 cells to better migrate from the scaffold surface to the inner scaffold structure. Cell migration into the bulk volume of the scaffold is an essential condition for the successful integration of the scaffold into the surrounding tissue [78]. Therefore, the decrease in density of 3T3-L1 cells with an increasing PLGA concentration in the electrospinning solutions may be a positive factor indicating the possibility of cell migration into the bulk volume of the scaffold. Nevertheless, it should be considered that cell proliferation in the case of PLGA scaffolds may not change [23], or may increase [19] with the increase in PLGA concentration in the electrospinning solutions and the corresponding increase in fiber diameter. Therefore, to evaluate the effect of polymer concentration on the biological properties of scaffolds, it is necessary to investigate not only how the fiber diameter changes, but also how the pore size, porosity, fiber orientation, etc., change. The decrease in cell density on PLGA scaffolds with increasing polymer concentrations in the electrospinning solutions could be related to a decrease in porosity [42]. For these reasons, the lowest cell density was observed for the 5% PLGA scaffold samples with the highest average fiber diameters (Figure 3) and the lowest porosity values (SI Figure S2). These findings could also explain why the optical density did not change with increasing PLGA electrospinning solution concentration (Figure 5a). This is due to the fact that only extracts of PLGA samples were studied, which can only be used for the analysis of toxic substances in scaffolds their morphological differences are not taken into account, which are essential factors relating to cell adhesion and proliferative activity.

Nevertheless, it is important to understand that the dependence of biological properties on the morphology of scaffolds is multifactorial, since a large number of different factors such as fiber diameter, pore size, porosity, etc., have to be considered [77]. Therefore, there are research articles in which the non-corresponding dependencies of biological properties on the diameter of electrospun scaffold fibers have been investigated [79–81].

5. Conclusions

Poly(lactide-co-glycolide) scaffolds were fabricated via electrospinning from electrospinning solutions containing four different concentrations of poly(lactide-co-glycolide) (2 wt.%, 3 wt.%, 4 wt.%, and 5 wt.%). With increasing concentrations of poly(lactide-co-glycolide), the viscosity of the electrospinning solutions increased from $169 \pm 10 \text{ mPa} \times \text{s}$ to $877 \pm 35 \text{ mPa} \times \text{s}$, the mean fiber diameter increased from $0.79 \pm 0.33 \mu\text{m}$ to $1.79 \pm 0.73 \mu\text{m}$, the micro-roughness increased from $713 \pm 88 \text{ nm}$ to $1394 \pm 208 \text{ nm}$, and the nano-roughness increased from $3.58 \pm 1.65 \text{ nm}$ to $17.67 \pm 4.19 \text{ nm}$. Unsurprisingly, the Raman spectra and X-ray diffraction patterns do not depend on the concentration of poly(lactide-co-glycolide) in the electrospinning solutions. The wettability does not change for all samples and is in the range of $125^\circ\text{--}129^\circ \pm 3^\circ$. Moreover, the tensile strength increases from $4.0 \pm 0.6 \text{ MPa}$ to $5.6 \pm 0.3 \text{ MPa}$, and the maximum elongation at break increases from $161\% \pm 17\%$ to $501\% \pm 24\%$. During the *in vitro* study to evaluate hydrolytic degradation, it was found that the mass, molecular weight and morphology of poly(lactide-co-glycolide) scaffold samples remained almost unchanged during 1, 2 or 3 months of being immersed in PBS, which is related to the high monomer ratio of lactic acid to glycolic acid and the high molecular weight of the copolymer poly(lactide-co-glycolide) being used. Examination of the biological properties revealed that all poly(lactide-co-glycolide) scaffold samples were not cytotoxic towards mouse 3T3-L1 embryonic fibroblasts, and that cell densities did not vary among the different scaffold samples. However, on the fifth day of the *in vitro* assays, a decrease in the number of cells was observed with an increasing concentration of poly(lactide-co-glycolide) in the electrospinning solutions from which the scaffolds were prepared. Poly(lactide-co-glycolide) scaffolds prepared from a 4 wt.% electrospinning solution exhibited optimal mechanical and biological properties and could be recommended for use in skin tissue regeneration. Such scaffolds prepared with 4 wt.% PLGA showed a mean fiber diameter of $1.36 \pm 0.46 \mu\text{m}$, a roughness in the scanning area of $40 \times 40 \mu\text{m}^2$ of $996 \pm 153 \text{ nm}$, a porosity of $80\% \pm 5\%$, a tensile strength of $5.5 \pm 0.3 \text{ MPa}$, a maximum elongation at break of $353\% \pm 15\%$, and a cell density of $1038 \pm 63 \text{ cells}/\text{mm}^2$

obtained at the fifth day of the in vitro assay. In comparison, scaffolds fabricated with 2 wt.% and 3 wt.% poly(lactide-co-glycolide) showed a tensile strength of 4.0 ± 0.6 MPa and 4.7 ± 0.2 MPa, and a maximum elongation at break of $161\% \pm 17\%$ and $244\% \pm 19\%$, respectively, which in turn is too low for skin tissue regeneration, making them unsuitable for this application. The scaffolds prepared with 5 wt.% poly(lactide-co-glycolide) showed an elongation at break value that is too high ($501\% \pm 24\%$). Additionally, these scaffolds prepared with 5 wt.% poly(lactide-co-glycolide) showed the lowest porosity ($74\% \pm 5\%$), which may have had a negative effect on their biological properties.

Supplementary Materials: The following supporting information can be downloaded at: <https://www.mdpi.com/article/10.3390/technologies11050137/s1>, Figure S1: Viscosity and of poly(lactide-co-glycolide) (PLGA) electrospinning solutions prepared with different concentrations of PLGA (2, 3, 4 and 5 wt.%) dissolved in hexafluoro-2-propanol (HFIP); Figure S2: Porosity of the poly(lactide-co-glycolide) (PLGA) scaffolds under investigation, measured by the gravimetric method (for more details, see chapter 2.5 in the main manuscript); Figure S3: Raman spectra of the studied poly(lactide-co-glycolide) (PLGA) scaffolds made from electrospinning solutions with different PLGA concentrations (2, 3, 4 and 5 wt.%) dissolved in hexafluoro-2-propanol (HFIP); Figure S4: X-ray diffractograms of poly(lactide-co-glycolide) (PLGA) scaffolds made from electrospinning solutions with different PLGA concentrations (2, 3, 4 and 5 wt.%) dissolved in hexafluoro-2-propanol (HFIP); Figure S5: Images of water droplets with the corresponding water contact angles after 2 s (top row) and after 1 min (bottom row) on the surface of poly(lactide-co-glycolide) (PLGA) scaffolds prepared from electrospinning solutions with different PLGA concentrations (2, 3, 4 and 5 wt.%) dissolved in hexafluoro-2-propanol (HFIP); Figure S6: Mechanical properties of the prepared poly(lactide-co-glycolide) (PLGA) scaffolds made from electrospinning solutions with different PLGA polymer concentrations (2, 3, 4 and 5 wt.%) dissolved in hexafluoro-2-propanol (HFIP): (a) tensile strength of the PLGA scaffolds under investigation and (b) maximum elongation at break; Figure S7: Relative remaining mass of poly(lactide-co-glycolide) (PLGA) scaffolds, prepared from electrospinning solutions with different polymer concentrations (2, 3, 4 and 5 wt.%) dissolved in hexafluoro-2-propanol (HFIP) and immersed in phosphate buffer saline (PBS) for 1, 2 or 3 months: (a) 2%, (b) 3%, (c) 4%, (d) 5%; Figure S8: Molecular weights (number average molecular weight (M_n) and molecular weight (M_w)) and molecular weight differences (ΔM_n , ΔM_w) of poly(lactide-co-glycolide) (PLGA) scaffolds prepared from electrospinning solutions with different PLGA concentrations (2, 3, 4 and 5 wt.%) dissolved in hexafluoro-2-propanol (HFIP), not immersed (Before PBS) and immersed in phosphate-buffered saline (PBS) for 1, 2 or 3 months: (a) M_n , (b) M_w (c) ΔM_n and (d) ΔM_w ; Figure S9: Scanning electron microscopy (SEM) micrographs at $1000\times$ magnification of poly(lactide-co-glycolide) (PLGA) scaffolds fabricated from electrospinning solutions with different PLGA concentrations (2, 3, 4 and 5 wt.%) and immersed in phosphate buffer saline (PBS) for 1, 2 or 3 months; Figure S10: Scanning electron microscopy (SEM) micrographs at $5000\times$ magnification of poly(lactide-co-glycolide) (PLGA) scaffolds fabricated from electrospinning solutions with different PLGA concentrations (2, 3, 4 and 5 wt.%) and immersed in phosphate buffer saline (PBS) for 1, 2 or 3 months.

Author Contributions: A.D.B.: investigation, writing—original draft, visualization; T.-H.T.: investigation; A.G.D.: investigation; E.V.P.: investigation; G.E.D.: investigation, validation; A.I.K.: writing—review & editing, validation; S.R.: writing—review & editing, supervision, validation; S.I.T.: conceptualization, supervision, project administration, funding acquisition. All authors have read and agreed to the published version of the manuscript.

Funding: This research was supported by the Ministry of Science and Higher Education of the Russian Federation, project Nauka FSWW-2023-0007.

Institutional Review Board Statement: Not applicable.

Informed Consent Statement: Not applicable.

Data Availability Statement: Data underlying the results presented in this paper are not publicly available at this time but may be obtained from the authors upon reasonable request.

Acknowledgments: This research was carried out using the equipment of the CSU NMNT, Common Use Center (CUC) of Tomsk Polytechnic University and the Resource Center “Materials Science Shared Center”, part of the “Tomsk Regional Common Use Center (TRCUC)” of Tomsk State University. The authors are grateful to A. A. Ditts for depositing a gold layer on the samples for SEM micrographs measurements and A. L. Zinoviev for the GPC measurements of the molecular weights of the PLGA scaffolds prepared.

Conflicts of Interest: The authors declare no conflict of interest.

References

1. Jun, I.; Han, H.-S.; Edwards, J.; Jeon, H. Electrospun Fibrous Scaffolds for Tissue Engineering: Viewpoints on Architecture and Fabrication. *Int. J. Mol. Sci.* **2018**, *19*, 745. [[CrossRef](#)]
2. Xie, X.; Chen, Y.; Wang, X.; Xu, X.; Shen, Y.; Khan, A.U.R.; Aldalbahi, A.; Fetz, A.E.; Bowlin, G.L.; El-Newehy, M.; et al. Electrospinning Nanofiber Scaffolds for Soft and Hard Tissue Regeneration. *J. Mater. Sci. Technol.* **2020**, *59*, 243–261. [[CrossRef](#)]
3. Chung, H.H.; Mireles, M.; Kwarta, B.J.; Gaborski, T.R. Use of Porous Membranes in Tissue Barrier and Co-Culture Models. *Lab Chip* **2018**, *18*, 1671–1689. [[CrossRef](#)]
4. Luraghi, A.; Peri, F.; Moroni, L. Electrospinning for Drug Delivery Applications: A Review. *J. Control. Release* **2021**, *334*, 463–484. [[CrossRef](#)] [[PubMed](#)]
5. Haider, A.; Haider, S.; Kang, I.-K. A Comprehensive Review Summarizing the Effect of Electrospinning Parameters and Potential Applications of Nanofibers in Biomedical and Biotechnology. *Arab. J. Chem.* **2018**, *11*, 1165–1188. [[CrossRef](#)]
6. Zhao, W.; Li, J.; Jin, K.; Liu, W.; Qiu, X.; Li, C. Fabrication of Functional PLGA-Based Electrospun Scaffolds and Their Applications in Biomedical Engineering. *Mater. Sci. Eng. C* **2016**, *59*, 1181–1194. [[CrossRef](#)] [[PubMed](#)]
7. Backes, E.H.; Harb, S.V.; Beatrice, C.A.G.; Shimomura, K.M.B.; Passador, F.R.; Costa, L.C.; Pessan, L.A. Polycaprolactone Usage in Additive Manufacturing Strategies for Tissue Engineering Applications: A Review. *J. Biomed. Mater. Res. Part B Appl. Biomater.* **2022**, *110*, 1479–1503. [[CrossRef](#)] [[PubMed](#)]
8. Santoro, M.; Shah, S.R.; Walker, J.L.; Mikos, A.G. Poly(Lactic Acid) Nanofibrous Scaffolds for Tissue Engineering. *Adv. Drug Deliv. Rev.* **2016**, *107*, 206–212. [[CrossRef](#)]
9. Kim, H.Y.; Kim, H.N.; Lee, S.J.; Song, J.E.; Kwon, S.Y.; Chung, J.W.; Lee, D.; Khang, G. Effect of Pore Sizes of PLGA Scaffolds on Mechanical Properties and Cell Behaviour for Nucleus Pulposus Regeneration in Vivo. *J. Tissue Eng. Regen. Med.* **2017**, *11*, 44–57. [[CrossRef](#)]
10. Keirouz, A.; Chung, M.; Kwon, J.; Fortunato, G.; Radacsi, N. 2D and 3D Electrospinning Technologies for the Fabrication of Nanofibrous Scaffolds for Skin Tissue Engineering: A Review. *WIREs Nanomed. Nanobiotechnol.* **2020**, *12*, e01626. [[CrossRef](#)]
11. Keshvardoostchokami, M.; Majidi, S.S.; Huo, P.; Ramachandran, R.; Chen, M.; Liu, B. Electrospun Nanofibers of Natural and Synthetic Polymers as Artificial Extracellular Matrix for Tissue Engineering. *Nanomaterials* **2020**, *11*, 21. [[CrossRef](#)]
12. Unal, S.; Arslan, S.; Yilmaz, B.K.; Oktar, F.N.; Ficali, D.; Ficali, A.; Gunduz, O. Polycaprolactone/Gelatin/Hyaluronic Acid Electrospun Scaffolds to Mimic Glioblastoma Extracellular Matrix. *Materials* **2020**, *13*, 2661. [[CrossRef](#)]
13. Mombini, S.; Mohammadnejad, J.; Bakhshandeh, B.; Narmani, A.; Nourmohammadi, J.; Vahdat, S.; Zirak, S. Chitosan-PVA-CNT Nanofibers as Electrically Conductive Scaffolds for Cardiovascular Tissue Engineering. *Int. J. Biol. Macromol.* **2019**, *140*, 278–287. [[CrossRef](#)] [[PubMed](#)]
14. Boni, R.; Ali, A.; Shavandi, A.; Clarkson, A.N. Current and Novel Polymeric Biomaterials for Neural Tissue Engineering. *J. Biomed. Sci.* **2018**, *25*, 90. [[CrossRef](#)] [[PubMed](#)]
15. He, P.; Zhong, Q.; Ge, Y.; Guo, Z.; Tian, J.; Zhou, Y.; Ding, S.; Li, H.; Zhou, C. Dual Drug Loaded Coaxial Electrospun PLGA/PVP Fiber for Guided Tissue Regeneration under Control of Infection. *Mater. Sci. Eng. C* **2018**, *90*, 549–556. [[CrossRef](#)] [[PubMed](#)]
16. Jin, S.; Xia, X.; Huang, J.; Yuan, C.; Zuo, Y.; Li, Y.; Li, J. Recent Advances in PLGA-Based Biomaterials for Bone Tissue Regeneration. *Acta Biomater.* **2021**, *127*, 56–79. [[CrossRef](#)]
17. Zhao, J.; Han, F.; Zhang, W.; Yang, Y.; You, D.; Li, L. Toward Improved Wound Dressings: Effects of Polydopamine-Decorated Poly(Lactic-Co-Glycolic Acid) Electrospinning Incorporating Basic Fibroblast Growth Factor and Ponericin G1. *RSC Adv.* **2019**, *9*, 33038–33051. [[CrossRef](#)]
18. Zhao, L.; He, C.; Gao, Y.; Cen, L.; Cui, L.; Cao, Y. Preparation and Cytocompatibility of PLGA Scaffolds with Controllable Fiber Morphology and Diameter Using Electrospinning Method. *J. Biomed. Mater. Res. Part B Appl. Biomater.* **2008**, *87B*, 26–34. [[CrossRef](#)]
19. Narayanan, N.; Jiang, C.; Wang, C.; Uzunalli, G.; Whittern, N.; Chen, D.; Jones, O.G.; Kuang, S.; Deng, M. Harnessing Fiber Diameter-Dependent Effects of Myoblasts Toward Biomimetic Scaffold-Based Skeletal Muscle Regeneration. *Front. Bioeng. Biotechnol.* **2020**, *8*, 203. [[CrossRef](#)]
20. Mo, X.; Xu, C.; Kotaki, M.; Ramakrishna, S. Electrospun P(LLA-CL) Nanofiber: A Biomimetic Extracellular Matrix for Smooth Muscle Cell and Endothelial Cell Proliferation. *Biomaterials* **2004**, *25*, 1883–1890. [[CrossRef](#)]
21. Tarus, B.; Fadel, N.; Al-Oufy, A.; El-Messiry, M. Effect of Polymer Concentration on the Morphology and Mechanical Characteristics of Electrospun Cellulose Acetate and Poly (Vinyl Chloride) Nanofiber Mats. *Alex. Eng. J.* **2016**, *55*, 2975–2984. [[CrossRef](#)]

22. Rashid, T.U.; Gorga, R.E.; Krause, W.E. Mechanical Properties of Electrospun Fibers—A Critical Review. *Adv. Eng. Mater.* **2021**, *23*, 2100153. [[CrossRef](#)]
23. Vashaghian, M.; Zandieh-Doulabi, B.; Roovers, J.-P.; Smit, T.H. Electrospun Matrices for Pelvic Floor Repair: Effect of Fiber Diameter on Mechanical Properties and Cell Behavior. *Tissue Eng. Part A* **2016**, *22*, 1305–1316. [[CrossRef](#)] [[PubMed](#)]
24. Schneider, C.A.; Rasband, W.S.; Eliceiri, K.W. NIH Image to ImageJ: 25 Years of Image Analysis. *Nat. Methods* **2012**, *9*, 671–675. [[CrossRef](#)] [[PubMed](#)]
25. Yang Yu, B.; Elbuken, C.; Ren, C.L.; Huissoon, J.P. Image Processing and Classification Algorithm for Yeast Cell Morphology in a Microfluidic Chip. *J. Biomed. Opt.* **2011**, *16*, 066008. [[CrossRef](#)] [[PubMed](#)]
26. Hotaling, N.A.; Bharti, K.; Kriel, H.; Simon, C.G. DiameterJ: A Validated Open Source Nanofiber Diameter Measurement Tool. *Biomaterials* **2015**, *61*, 327–338. [[CrossRef](#)]
27. Peillon, S.; Autricque, A.; Redolfi, M.; Stancu, C.; Gensdarmes, F.; Grisolia, C.; Pluchery, O. Adhesion of Tungsten Particles on Rough Tungsten Surfaces Using Atomic Force Microscopy. *J. Aerosol Sci.* **2019**, *137*, 105431. [[CrossRef](#)]
28. Nečas, D.; Klapetek, P. Gwyddion: An Open-Source Software for SPM Data Analysis. *Open Phys.* **2012**, *10*, 181–188. [[CrossRef](#)]
29. Loh, Q.L.; Choong, C. Three-Dimensional Scaffolds for Tissue Engineering Applications: Role of Porosity and Pore Size. *Tissue Eng. Part B Rev.* **2013**, *19*, 485–502. [[CrossRef](#)]
30. Kemme, M.; Heinzel-Wieland, R. Quantitative Assessment of Antimicrobial Activity of PLGA Films Loaded with 4-Hexylresorcinol. *J. Funct. Biomater.* **2018**, *9*, 4. [[CrossRef](#)]
31. BS EN ISO 10993-13:2010; International Standard EN ISO 10993-13:2010—Biological Evaluation of Medical Devices. Part 13: Identification and Quantification of Degradation Products from Polymeric Medical Devices. International Organization for Standardization: London, UK, 2010.
32. Yang, Y.; Zhao, Y.; Tang, G.; Li, H.; Yuan, X.; Fan, Y. In Vitro Degradation of Porous Poly(L-Lactide-Co-Glycolide)/ β -Tricalcium Phosphate (PLGA/ β -TCP) Scaffolds under Dynamic and Static Conditions. *Polym. Degrad. Stab.* **2008**, *93*, 1838–1845. [[CrossRef](#)]
33. Vakilian, S.; Norouzi, M.; Soufi-Zomorrod, M.; Shabani, I.; Hosseinzadeh, S.; Soleimani, M.L. Inermis -Loaded Nanofibrous Scaffolds for Wound Dressing Applications. *Tissue Cell* **2018**, *51*, 32–38. [[CrossRef](#)] [[PubMed](#)]
34. Preethi, G.U.; Unnikrishnan, B.S.; Sreekutty, J.; Archana, M.G.; Anupama, M.S.; Shiji, R.; Raveendran Pillai, K.; Joseph, M.M.; Syama, H.P.; Sreelekha, T.T. Semi-Interpenetrating Nanosilver Doped Polysaccharide Hydrogel Scaffolds for Cutaneous Wound Healing. *Int. J. Biol. Macromol.* **2020**, *142*, 712–723. [[CrossRef](#)] [[PubMed](#)]
35. Kamiloglu, S.; Sari, G.; Ozdal, T.; Capanoglu, E. Guidelines for Cell Viability Assays. *Food Front.* **2020**, *1*, 332–349. [[CrossRef](#)]
36. Tiwari, S.K.; Venkatraman, S.S. Importance of Viscosity Parameters in Electrospinning: Of Monolithic and Core-Shell Fibers. *Mater. Sci. Eng. C* **2012**, *32*, 1037–1042. [[CrossRef](#)]
37. Liu, X.; Baldursdottir, S.G.; Aho, J.; Qu, H.; Christensen, L.P.; Rantanen, J.; Yang, M. Electrospinnability of Poly Lactic-Co-Glycolic Acid (PLGA): The Role of Solvent Type and Solvent Composition. *Pharm. Res.* **2017**, *34*, 738–749. [[CrossRef](#)]
38. Sill, T.J.; von Recum, H.A. Electrospinning: Applications in Drug Delivery and Tissue Engineering. *Biomaterials* **2008**, *29*, 1989–2006. [[CrossRef](#)]
39. Hossain, M.F.; Gong, R.H.; Rigout, M. Effect of Polymer Concentration on Electrospinning of Hydroxypropyl- β -Cyclodextrins/PEO Nanofibres. *J. Text. Inst.* **2016**, *107*, 1511–1518. [[CrossRef](#)]
40. Christopherson, G.T.; Song, H.; Mao, H.-Q. The Influence of Fiber Diameter of Electrospun Substrates on Neural Stem Cell Differentiation and Proliferation. *Biomaterials* **2009**, *30*, 556–564. [[CrossRef](#)]
41. Han, D.G.; Ahn, C.B.; Lee, J.-H.; Hwang, Y.; Kim, J.H.; Park, K.Y.; Lee, J.W.; Son, K.H. Optimization of Electrospun Poly(Caprolactone) Fiber Diameter for Vascular Scaffolds to Maximize Smooth Muscle Cell Infiltration and Phenotype Modulation. *Polymers* **2019**, *11*, 643. [[CrossRef](#)]
42. Soliman, S.; Sant, S.; Nichol, J.W.; Khabiry, M.; Traversa, E.; Khademhosseini, A. Controlling the Porosity of Fibrous Scaffolds by Modulating the Fiber Diameter and Packing Density. *J. Biomed. Mater. Res. Part A* **2011**, *96A*, 566–574. [[CrossRef](#)]
43. Guo, Z.; Ma, M.; Huang, X.; Li, H.; Zhou, C. Effect of Fiber Diameter on Proliferation and Differentiation of MC3T3-E1 Pre-Osteoblasts. *J. Biomater. Tissue Eng.* **2017**, *7*, 162–169. [[CrossRef](#)]
44. Rnjak-Kovacina, J.; Weiss, A.S. Increasing the Pore Size of Electrospun Scaffolds. *Tissue Eng. Part B Rev.* **2011**, *17*, 365–372. [[CrossRef](#)]
45. Yu, C.-C.; Chen, Y.-W.; Yeh, P.-Y.; Hsiao, Y.-S.; Lin, W.-T.; Kuo, C.-W.; Chueh, D.-Y.; You, Y.-W.; Shyue, J.-J.; Chang, Y.-C.; et al. Random and Aligned Electrospun PLGA Nanofibers Embedded in Microfluidic Chips for Cancer Cell Isolation and Integration with Air Foam Technology for Cell Release. *J. Nanobiotechnol.* **2019**, *17*, 31. [[CrossRef](#)]
46. Dillen, K.; Vandervoort, J.; Van den Mooter, G.; Verheyden, L.; Ludwig, A. Factorial Design, Physicochemical Characterisation and Activity of Ciprofloxacin-PLGA Nanoparticles. *Int. J. Pharm.* **2004**, *275*, 171–187. [[CrossRef](#)] [[PubMed](#)]
47. Blasi, P. Poly(Lactic Acid)/Poly(Lactic-Co-Glycolic Acid)-Based Microparticles: An Overview. *J. Pharm. Investig.* **2019**, *49*, 337–346. [[CrossRef](#)]
48. Makadia, H.K.; Siegel, S.J. Poly Lactic-Co-Glycolic Acid (PLGA) as Biodegradable Controlled Drug Delivery Carrier. *Polymers* **2011**, *3*, 1377–1397. [[CrossRef](#)] [[PubMed](#)]
49. Dai, J.; Liang, M.; Zhang, Z.; Bernaerts, K.V.; Zhang, T. Synthesis and Crystallization Behavior of Poly (Lactide-Co-Glycolide). *Polymer* **2021**, *235*, 124302. [[CrossRef](#)]

50. Gentile, P.; Chiono, V.; Carmagnola, I.; Hatton, P. An Overview of Poly(Lactic-Co-Glycolic) Acid (PLGA)-Based Biomaterials for Bone Tissue Engineering. *Int. J. Mol. Sci.* **2014**, *15*, 3640–3659. [[CrossRef](#)]
51. Lanao, R.P.F.; Jonker, A.M.; Wolke, J.G.C.; Jansen, J.A.; van Hest, J.C.M.; Leeuwenburgh, S.C.G. Physicochemical Properties and Applications of Poly(Lactic-Co-Glycolic Acid) for Use in Bone Regeneration. *Tissue Eng. Part B Rev.* **2013**, *19*, 380–390. [[CrossRef](#)]
52. Sadeghi, A.R.; Nokhasteh, S.; Molavi, A.M.; Khorsand-Ghayeni, M.; Naderi-Meshkin, H.; Mahdizadeh, A. Surface Modification of Electrospun PLGA Scaffold with Collagen for Bioengineered Skin Substitutes. *Mater. Sci. Eng. C* **2016**, *66*, 130–137. [[CrossRef](#)] [[PubMed](#)]
53. Bazgir, M.; Zhang, W.; Zhang, X.; Elies, J.; Saeinasab, M.; Coates, P.; Youseffi, M.; Sefat, F. Degradation and Characterisation of Electrospun Polycaprolactone (PCL) and Poly(Lactic-Co-Glycolic Acid) (PLGA) Scaffolds for Vascular Tissue Engineering. *Materials* **2021**, *14*, 4773. [[CrossRef](#)] [[PubMed](#)]
54. Simonet, M.; Stingelin, N.; Wismans, J.G.F.; Oomens, C.W.J.; Driessen-Mol, A.; Baaijens, F.P.T. Tailoring the Void Space and Mechanical Properties in Electrospun Scaffolds towards Physiological Ranges. *J. Mater. Chem. B* **2014**, *2*, 305–313. [[CrossRef](#)]
55. Can-Herrera, L.A.; Oliva, A.I.; Dzul-Cervantes, M.A.A.; Pacheco-Salazar, O.F.; Cervantes-Uc, J.M. Morphological and Mechanical Properties of Electrospun Polycaprolactone Scaffolds: Effect of Applied Voltage. *Polymers* **2021**, *13*, 662. [[CrossRef](#)]
56. Chew, S.Y.; Hufnagel, T.C.; Lim, C.T.; Leong, K.W. Mechanical Properties of Single Electrospun Drug-Encapsulated Nanofibres. *Nanotechnology* **2006**, *17*, 3880–3891. [[CrossRef](#)] [[PubMed](#)]
57. Papkov, D.; Zou, Y.; Andalib, M.N.; Goponenko, A.; Cheng, S.Z.D.; Dzenis, Y.A. Simultaneously Strong and Tough Ultrafine Continuous Nanofibers. *ACS Nano* **2013**, *7*, 3324–3331. [[CrossRef](#)]
58. Zhao, H.; Li, L.; Ding, S.; Liu, C.; Ai, J. Effect of Porous Structure and Pore Size on Mechanical Strength of 3D-Printed Comby Scaffolds. *Mater. Lett.* **2018**, *223*, 21–24. [[CrossRef](#)]
59. Ikeda, R.; Fujioka, H.; Nagura, I.; Kokubu, T.; Toyokawa, N.; Inui, A.; Makino, T.; Kaneko, H.; Doita, M.; Kurosaka, M. The Effect of Porosity and Mechanical Property of a Synthetic Polymer Scaffold on Repair of Osteochondral Defects. *Int. Orthop.* **2009**, *33*, 821–828. [[CrossRef](#)] [[PubMed](#)]
60. Ghosh, S.; Gutierrez, V.; Fernández, C.; Rodriguez-Perez, M.A.; Viana, J.C.; Reis, R.L.; Mano, J.F. Dynamic Mechanical Behavior of Starch-Based Scaffolds in Dry and Physiologically Simulated Conditions: Effect of Porosity and Pore Size. *Acta Biomater.* **2008**, *4*, 950–959. [[CrossRef](#)]
61. Suamte, L.; Tirkey, A.; Barman, J.; Jayasekhar Babu, P. Various Manufacturing Methods and Ideal Properties of Scaffolds for Tissue Engineering Applications. *Smart Mater. Manuf.* **2023**, *1*, 100011. [[CrossRef](#)]
62. Joodaki, H.; Panzer, M.B. Skin Mechanical Properties and Modeling: A Review. *Proc. Inst. Mech. Eng. Part H J. Eng. Med.* **2018**, *232*, 323–343. [[CrossRef](#)]
63. Wu, X.S.; Wang, N. Synthesis, Characterization, Biodegradation, and Drug Delivery Application of Biodegradable Lactic/Glycolic Acid Polymers. Part II: Biodegradation. *J. Biomater. Sci. Polym. Ed.* **2001**, *12*, 21–34. [[CrossRef](#)]
64. Shin, H.J.; Lee, C.H.; Cho, I.H.; Kim, Y.-J.; Lee, Y.-J.; Kim, I.A.; Park, K.-D.; Yui, N.; Shin, J.-W. Electrospun PLGA Nanofiber Scaffolds for Articular Cartilage Reconstruction: Mechanical Stability, Degradation and Cellular Responses under Mechanical Stimulation in Vitro. *J. Biomater. Sci. Polym. Ed.* **2006**, *17*, 103–119. [[CrossRef](#)] [[PubMed](#)]
65. Mehra, M.; Asadollahi, M.A.; Nasri-Nasrabadi, B.; Ghaedi, K.; Salehi, H.; Dolatshahi-Pirouz, A.; Arpanaei, A. Incorporation of Mesoporous Silica Nanoparticles into Random Electrospun PLGA and PLGA/Gelatin Nanofibrous Scaffolds Enhances Mechanical and Cell Proliferation Properties. *Mater. Sci. Eng. C* **2016**, *66*, 25–32. [[CrossRef](#)] [[PubMed](#)]
66. You, Y.; Min, B.-M.; Lee, S.J.; Lee, T.S.; Park, W.H. In Vitro Degradation Behavior of Electrospun Polyglycolide, Polylactide, and Poly(Lactide-Co-Glycolide). *J. Appl. Polym. Sci.* **2005**, *95*, 193–200. [[CrossRef](#)]
67. Saha, S.K.; Tsuji, H. Effects of Molecular Weight and Small Amounts of D-Lactide Units on Hydrolytic Degradation of Poly(L-Lactic Acid). *S. Polym. Degrad. Stab.* **2006**, *91*, 1665–1673. [[CrossRef](#)]
68. de Boer, R.; Knight, A.M.; Borntraeger, A.; Hébert-Blouin, M.-N.; Spinner, R.J.; Malessy, M.J.A.; Yaszemski, M.J.; Windebank, A.J. Rat Sciatic Nerve Repair with a Poly-Lactic-Co-Glycolic Acid Scaffold and Nerve Growth Factor Releasing Microspheres. *Microsurgery* **2011**, *31*, 293–302. [[CrossRef](#)] [[PubMed](#)]
69. Graziano, A.; D’Aquino, R.; Cusella-De Angelis, M.G.; Laino, G.; Piattelli, A.; Pacifici, M.; De Rosa, A.; Papaccio, G. Concave Pit-Containing Scaffold Surfaces Improve Stem Cell-Derived Osteoblast Performance and Lead to Significant Bone Tissue Formation. *PLoS ONE* **2007**, *2*, e496. [[CrossRef](#)] [[PubMed](#)]
70. Ginjupalli, K.; Averineni, R.K.; Shavi, G.V.; Armugam, K.; Bhat, M.N.U.; Meka, S.R. Biodegradable Composite Scaffolds of Poly(Lactic-co-glycolic Acid) 85:15 and Nano-hydroxyapatite with Acidic Microclimate Controlling Additive. *Polym. Compos.* **2017**, *38*, 1175–1182. [[CrossRef](#)]
71. Blackwood, K.A.; McKean, R.; Canton, I.; Freeman, C.O.; Franklin, K.L.; Cole, D.; Brook, I.; Farthing, P.; Rimmer, S.; Haycock, J.W.; et al. Development of Biodegradable Electrospun Scaffolds for Dermal Replacement. *Biomaterials* **2008**, *29*, 3091–3104. [[CrossRef](#)]
72. Chor, A.; Gonçalves, R.P.; Costa, A.M.; Farina, M.; Ponche, A.; Sirelli, L.; Schrodj, G.; Gree, S.; de Andrade, L.R.; Anselme, K.; et al. In Vitro Degradation of Electrospun Poly(Lactic-Co-Glycolic Acid) (PLGA) for Oral Mucosa Regeneration. *Polymers* **2020**, *12*, 1853. [[CrossRef](#)] [[PubMed](#)]
73. Gao, J.; Chen, S.; Tang, D.; Jiang, L.; Shi, J.; Wang, S. Mechanical Properties and Degradability of Electrospun PCL/PLGA Blended Scaffolds as Vascular Grafts. *Trans. Tianjin Univ.* **2019**, *25*, 152–160. [[CrossRef](#)]

74. Dias, J.R.; Sousa, A.; Augusto, A.; Bártolo, P.J.; Granja, P.L. Electrospun Polycaprolactone (PCL) Degradation: An In Vitro and In Vivo Study. *Polymers* **2022**, *14*, 3397. [[CrossRef](#)]
75. Chor, A.; Takiya, C.M.; Dias, M.L.; Gonçalves, R.P.; Petithory, T.; Cypriano, J.; de Andrade, L.R.; Farina, M.; Anselme, K. In Vitro and In Vivo Cell-Interactions with Electrospun Poly (Lactic-Co-Glycolic Acid) (PLGA): Morphological and Immune Response Analysis. *Polymers* **2022**, *14*, 4460. [[CrossRef](#)]
76. Kazemi, L.; Rahbarghazi, R.; Salehi, R.; Abedelahi, A.; Niari, S.A.; Karimipour, M.; Nasrabadi, H.T. Superior Synaptogenic Effect of Electrospun PLGA-PEG Nanofibers Versus PLGA Nanofibers on Human Neural SH-SY5Y Cells in a Three-Dimensional Culture System. *J. Mol. Neurosci.* **2020**, *70*, 1967–1976. [[CrossRef](#)]
77. Szentivanyi, A.; Chakradeo, T.; Zernetsch, H.; Glasmacher, B. Electrospun Cellular Microenvironments: Understanding Controlled Release and Scaffold Structure. *Adv. Drug Deliv. Rev.* **2011**, *63*, 209–220. [[CrossRef](#)] [[PubMed](#)]
78. Wu, J.; Hong, Y. Enhancing Cell Infiltration of Electrospun Fibrous Scaffolds in Tissue Regeneration. *Bioact. Mater.* **2016**, *1*, 56–64. [[CrossRef](#)]
79. Boudriot, U.; Dersch, R.; Greiner, A.; Wendorff, J.H. Electrospinning Approaches Toward Scaffold Engineering? A Brief Overview. *Artif. Organs* **2006**, *30*, 785–792. [[CrossRef](#)]
80. Badami, A.S.; Kreke, M.R.; Thompson, M.S.; Riffle, J.S.; Goldstein, A.S. Effect of Fiber Diameter on Spreading, Proliferation, and Differentiation of Osteoblastic Cells on Electrospun Poly(Lactic Acid) Substrates. *Biomaterials* **2006**, *27*, 596–606. [[CrossRef](#)]
81. Bashur, C.A.; Dahlgren, L.A.; Goldstein, A.S. Effect of Fiber Diameter and Orientation on Fibroblast Morphology and Proliferation on Electrospun Poly(d,l-Lactic-Co-Glycolic Acid) Meshes. *Biomaterials* **2006**, *27*, 5681–5688. [[CrossRef](#)]

Disclaimer/Publisher’s Note: The statements, opinions and data contained in all publications are solely those of the individual author(s) and contributor(s) and not of MDPI and/or the editor(s). MDPI and/or the editor(s) disclaim responsibility for any injury to people or property resulting from any ideas, methods, instructions or products referred to in the content.